Contributions of Fine and Coarse Particles to Light Absorption at an Urban Traffic Site during Street Dust Season

Luis M. F. Barreira[1], Delun Li[1], Jussi Hoivala[2], Minna Aurela[1], Aki Virkkula[1], Jarkko V. Niemi[3], Hanna E. Manninen[3], Topi Rönkkö[2], Hilkka Timonen[1], Sanna Saarikoski[1],

[1]Atmospheric Composition Research, Finnish Meteorological Institute, 00101, Helsinki, Finland
[2]Aerosol Physics Laboratory, Physics Unit, Faculty of Engineering and Natural Sciences, Tampere University, 33014, Tampere, Finland
[3]Helsinki Region Environmental Services Authority, 00066, Helsinki, Finland

Correspondence to: Luis M. F. Barreira (luis.barreira@fmi.fi)

Abstract. Light absorption by urban aerosols is dominated by fine particles (particulate matter ≤2.5 μm; $PM_{2.5}$), particularly from traffic exhaust and residential combustion. However, coarse particles (2.5–10 μm; $PM_{2.5-10}$) can also contribute during spring street dust events in northern countries, while coarse-mode absorption remains poorly constrained in climate and air-quality models. This study investigated size-resolved optical properties and chemical composition of PM in an urban street canyon during spring. Hourly PM_{10} concentrations averaged 27.1 μg m^{-3}, while $PM_{2.5}$ and PM_1 (≤1 μm) concentrations averaged 7.1 and 4.3 μg m^{-3}, respectively. Light absorption across PM_1, $PM_{2.5}$, and $PM_{7.2}$ fractions was dominated by submicron particles, predominantly at short wavelengths, while coarse particles enhanced absorption during dust-resuspension events. Equivalent black carbon (eBC) showed strong size dependence, with PM_1 capturing most combustion-derived BC and hourly eBC increasing by 14% in $PM_{2.5}$ and 41% in $PM_{7.2}$. Absorption Ångström exponent analysis revealed size- and source-dependent spectral differences, with stronger wavelength dependence during high PM_{10} dust events and values closer to unity under traffic-exhaust-dominated conditions. The inclusion of coarse particles complicated the interpretation of the $AAE_{470/950}$ and related biomass burning contribution estimates. Elemental analysis revealed elevated concentrations of Si, Fe, and Al in coarse PM, suggesting contributions from crustal material and/or non-exhaust emissions that may also influence optical properties. These findings demonstrate that quantification and source identification of urban aerosol light absorption requires consideration of the selected particle size cut-off.

1 Introduction

Atmospheric particulate matter (PM) is a key component influencing air quality, human health, and climate forcing due to its ability to absorb and scatter solar radiation. Fine particles ($D_p \leq 2.5$ µm), particularly those with diameter smaller than or equal to 1 µm (PM_1), are typically dominated by combustion-derived aerosols such as black carbon (BC) and secondary organic aerosols (SOA) (e.g. Barreira et al., 2021; Chen et al., 2022). These submicron particles are well known for their light-absorbing properties, primarily due to black carbon and to a lesser extent other absorbing components, which contribute to radiative forcing (e.g. Peng et al., 2016; Rovira et al., 2025). Coarse particles (2.5-10 µm), by contrast, have traditionally been considered less important for optical absorption and more relevant for scattering. However, recent evidence suggests that coarse-mode particles may also contribute to light absorption (e.g. Banerji et al., 2025), challenging the assumption that particle fractions larger than PM_1 play a negligible role in aerosol absorption properties.

The chemical composition of particulate matter plays a critical role in determining its light-absorbing properties. Different compounds exhibit varying degrees of sp^2 hybridization and molecular structures, leading to variability in their optical behavior (e.g. Kahnert and Kanngießer, 2020). In particular, the presence of carbonaceous material with sp^2 hybridization, such as in BC or certain polyaromatic compounds, strongly influences absorption (Bond and Bergstrom, 2006; Kahnert and Kanngießer, 2020). Furthermore, metal-rich particles and organic precursors catalyzed e.g. by iron have been shown to contribute to enhanced light absorption at certain wavelengths (e.g. Al-Abadleh et al., 2022, 2023; Lüchtrath et al., 2025). In addition to chemical composition, particle size, shape, morphology, density, and mixing state are important determinants of light absorption. Submicron particles generally absorb light more efficiently per unit mass due to their carbonaceous composition, whereas coarse particles, including mineral dust, can influence absorption when containing or being mixed with BC, iron oxides or other light-absorbing minerals, and light-absorbing organic matter (e.g. Wang et al., 2022; Zhang et al., 2008). In addition, particle size and mixing state influence both the magnitude and wavelength dependence of light absorption (e.g. Virkkula, 2021). The combination of chemical composition and physical properties ultimately controls how atmospheric particles interact with solar radiation across different wavelengths, highlighting the need to consider both particle composition and size when assessing PM optical effects.

Non-exhaust sources, including direct emissions from asphalt wear as well as resuspended road dust, brake wear, and tire wear, produce particles primarily in the coarse particle size range (e.g. Thorpe and Harrison, 2008; Wei and Kumar, 2024). Resuspended road dust represents a complex mixture of materials originating from multiple sources (e.g., asphalt, tire and brake wear, soil dust, and winter road maintenance materials), and these particles are often enriched in metals such as iron, copper, and zinc, as well as their corresponding oxides (e.g. Wagner et al., 2024). Tyre and brake wear particles contain also material that can absorb in BC wavelength, such as carbon black in tyres (e.g. Lee et al., 2025; Reynolds et al., 2024) and graphite in brake pads (e.g. Lyu and Olofsson, 2020). Recent studies have shown that non-exhaust emissions can constitute a significant fraction of dust- and traffic related PM mass (e.g. Kakavas and Pandis, 2021; Zhang et al., 2025), and these contributions are expected to increase further as vehicle fleets transition toward electrification and tailpipe emissions decline.

Despite these observations, the optical properties of these coarse particles remain poorly quantified, and it remains unclear how coarse-mode absorbers influence overall PM light absorption and derived BC concentrations.

Characterizing aerosol light absorption as a function of particle size and composition remains challenging due to instrumental limitations and methodological inconsistencies. Filter-based absorption photometers, such as multi-angle absorption photometers (MAAP) and aethalometers (e.g., AE33), are widely used to quantify equivalent black carbon (eBC) (e.g. Helin et al., 2018; Hernández et al., 2025; Luoma et al., 2021; Zioła et al., 2021). However, in practice, these instruments are typically operated with PM_1 or $PM_{2.5}$ size-selective inlets, reflecting both the predominantly submicron nature of black carbon and common air quality monitoring conventions (e.g. Barreira et al., 2021; Hernández et al., 2025; Malik and Aggarwal, 2021). As a result, absorption by coarse-mode particles may be systematically underrepresented. Coarse particles also exhibit different chemical composition from fine particles but the real-time characterization of coarse particles is more challenging as e.g. aerosol mass spectrometers (AMS) are generally limited to submicron particles (e.g. Canagaratna et al., 2007; Jayne et al., 2000). In addition, different monitoring networks and measurement platforms, such as ACTRIS and other regional or national air quality networks, often target different particle size fractions, which complicates intercomparisons and harmonization of datasets (e.g. ACTRIS, 2024; Zheng et al., 2025). Consequently, differences in sampling practices may limit the direct comparability of ambient eBC datasets and influence the determination of other relevant parameters such as the biomass burning fraction (BB%). The variability in eBC datasets caused by different sampling fractions also affects the emission factors determined using eBC measurements (e.g. Kozawa et al., 2014; Rönkkö et al., 2023; Saha et al., 2018). Consequently, this variability propagates to atmospheric models that use these emission factors to evaluate the impacts of emitted BC on air quality and climate.

To address these knowledge gaps, we conducted a dedicated field campaign to quantify the contributions of different particle sizes to urban aerosol light absorption during spring, when PM_{10} concentrations are typically elevated due to street dust resuspension events in northern countries (e.g. Barreira et al., 2021; Kupiainen et al., 2016; Stojiljkovic et al., 2019). Measurements were performed across several PM fractions using multiple complementary instruments: aethalometers for light absorption (PM_1, $PM_{2.5}$, and $PM_{7.2}$), XRF for elemental composition ($PM_{2.5}$, and PM_{10}), and an optical particle monitor for particle sizing and derived PM mass concentrations (PM_1, $PM_{2.5}$, and PM_{10}). To ensure that observed differences in light absorption across size fractions reflected true particle-size effects rather than instrument-specific biases, an intercomparison of the aethalometers and MAAP for PM_1 was also conducted. This integrated approach allowed us to quantify the relative contributions of different particle size fractions to light absorption under real-world urban conditions.

2 Experimental section

2.1 Measurement site

Traffic-influenced measurements were conducted at an urban supersite located within a characteristic street canyon in Helsinki, Finland (Mäkelänkatu 50) (e.g. Barreira et al., 2021). The observation period extended from 26 March to 2 May 2024. The street canyon consists of six traffic lanes, two tram tracks, and pedestrian walkways on both sides, with a total width of approximately 42 m. This location is commonly considered representative of a northern European urban traffic environment. On a typical weekday, around 17,000 vehicles travel along the street, with heavy-duty vehicles accounting for roughly 10 % according to municipal traffic statistics (City of Helsinki, unpublished data, 2025). Contributions from local biomass burning are negligible, as surrounding residential buildings rely primarily on district heating.

Following the main campaign, the intercomparison of the aethalometers and MAAP was conducted at the same site from 2 to 23 May 2024. This auxiliary campaign focused on evaluating consistency between three parallel instruments measuring aerosol absorption in different particulate size fractions (PM_1, $PM_{2.5}$, and $PM_{7.2}$). A detailed description of the instruments and methodology is provided in Sect. 2.2.

2.2 Instrumentation

2.2.1 Aethalometer (AE33)

In this study, aerosol light absorption in three particulate size fractions (PM_1, $PM_{2.5}$, and $PM_{7.2}$) was measured using three co-located AE33 aethalometers (Magee Scientific, Slovenia). The AE33 is a filter-based absorption photometer in which particles are collected on a moving filter tape, and light transmittance through the loaded filter is continuously recorded at seven wavelengths spanning the UV–Vis range (370, 470, 520, 590, 660, 880, and 950 nm) with a nominal full width at half maximum (FWHM) of about 20 nm and measured FWHM variance of 10–85 nm (e.g. Müller et al., 2011).

The AE33 reports eBC concentrations derived from light attenuation measurements (Magee Scientific, 2024). In this study, aerosol absorption coefficients $b_{abs}(\lambda)$ were calculated from the reported eBC concentrations and wavelength-dependent mass absorption cross-sections (MAC) using Eq. (1):

$$b_{abs}\,(\lambda) = MAC\,(\lambda) \times eBC\,(\lambda)\,, \quad (1)$$

where $MAC(\lambda)$ values were taken from the AE33 manufacturer specifications.

The absorption Ångström exponent (AAE), an important aerosol optical parameter used for aerosol characterization (e.g. Helin et al., 2021; Liu et al., 2018), was also calculated for different wavelengths using Eq. (2):

$$AAE_{\lambda_1/\lambda_2} = \frac{\ln(b_{abs}(\lambda_1)/b_{abs}(\lambda_2))}{\ln\,(\lambda_1/\lambda_2)}, \quad (2)$$

Absorption coefficients were hourly-averaged for AAE calculations to reduce uncertainty (e.g. Helin et al., 2021).

The AE33's in-built "Aethalometer model" also computes the percentage contribution of biomass burning, denoted as BB%, which is commonly defined by Eq. (3):

$$BB\% = 100\% \times \frac{\left(\frac{470}{950}\right)^{-AAE_{470/950}} - \left(\frac{470}{950}\right)^{-\alpha_{FF}}}{\left(\frac{470}{950}\right)^{-\alpha_{WB}} - \left(\frac{470}{950}\right)^{-\alpha_{FF}}}, \quad (3)$$

where α_{FF} and α_{WB} represent the AAE for fossil fuel and biomass-burning aerosols, respectively (Sandradewi et al., 2008). In the AE33 Aethalometer model, typical default values are $\alpha_{FF} = 1.0$ and $\alpha_{WB} = 2.0$. However, $\alpha_{FF} = 1.1$ for fossil fuel emissions and $\alpha_{WB} = 1.6$ for wood burning were applied in this article, since these values have been previously derived for the sampling site investigated in this study (Helin et al., 2018).

A source apportionment of $PM_{2.5\text{-}7.2}$ light absorption was performed using multiple linear regression analysis to assess the relationships between light absorption and elemental tracers associated with the PMF-derived source factors identified by Aurela et al. (2026). The predictors were selected based on their contribution and specificity to the PMF-derived source factors, together with their concentrations. Al, Cu, S, Na, and Cl were used as representative tracers of dust, non-exhaust emissions, combustion/secondary inorganic aerosol, aged salt, and fresh salt, respectively. Separate multiple linear regression models were fitted for light absorption at 370, 520, and 660 nm, with absorption at each wavelength used as the dependent variable and the five elemental tracers entered simultaneously as predictors. Model performance was assessed using the coefficient of determination (R^2), while the statistical significance of individual predictors was evaluated using regression coefficients, standard errors, t-statistics, and p-values. Multicollinearity among predictors was assessed using variance inflation factors (VIF) and tolerance values. Statistical analyses were performed using jamovi (Version 2.7.38; The jamovi project, 2026), an open-source statistical software platform. The relative contribution of each elemental tracer to light absorption was estimated by multiplying the mean concentration of each tracer over the measurement period by its corresponding regression-derived mass absorption efficiency (MAE) at each wavelength. The resulting tracer-specific absorption estimates were then normalized to the sum of the positive absorption contributions from all tracers to obtain their relative contributions to the regression-derived absorption. Negative regression-derived contributions were set to zero.

Filter-based absorption measurements are subject to several uncertainties, including multiple light scattering within the filter (e.g. Weingartner et al., 2003; Yus-Díez et al., 2021), loading effects as the filter accumulates particles (e.g. Drinovec et al., 2017; Virkkula et al., 2007; Weingartner et al., 2003), and apparent absorption from scattering aerosols (e.g. Arnott et al., 2005; Bond et al., 1999). The AE33 mitigates these artefacts through a dual-spot configuration, which corrects for loading effects and tape-advancement errors, improving the reliability of absorption measurements (Drinovec et al., 2015). However, no independent scattering measurements were available in this study to quantify potential multiple-scattering or scattering-related artefacts. These effects therefore cannot be separated from the measured absorption enhancement and represent an additional source of uncertainty when interpreting its magnitude.

For the main campaign, each AE33 was connected to a common sampling line with a blower proving a steady sample flow from outside. From that sampling line, each AE33 drew a separate sample flow, with flow rates determined by the cut-off diameters of the cyclone inlets used upstream of the AE33 instruments. PM_1, and $PM_{2.5}$ were obtained by using BGI model SCC-1.197 cyclone with the flow rates of 5 and 2 L min^{-1}, respectively, while $PM_{7.2}$ was obtained with BGI model SCC-1.829 cyclone with a flow rate of 2 L min^{-1}. Instruments operated with 1-minute time resolution. PTFE-coated glass fibre filter tapes

(Magee Scientific, type M8060) were used throughout the campaign. Absorption coefficients reported by the AE33 incorporate the manufacturer's multiple-scattering correction factor (C_{ref}=1.39) and wavelength-dependent mass absorption coefficients. During the intercomparison campaign, all three AE33 instruments measured light absorption in PM_1 using the same SCC-1.197 cyclone model mentioned above and operating simultaneously, enabling a direct assessment of the consistency and reproducibility of light-absorption measurements under identical aerosol conditions. The intercomparison data were also used to quantify the instrument-to-instrument uncertainty and to propagate this uncertainty to the incremental $PM_{1\text{-}2.5}$ and $PM_{2.5\text{-}7.2}$ absorption values, as described in the Supplementary Information (Sect. S2). The median eBC concentration measured by the three AE33 devices in PM_1 was 0.32 μg m^{-3} (Fig. S1). In addition to the AE33 measurements, eBC concentrations in PM_1 were intercompared with data from a Multi-Angle Absorption Photometer (MAAP; Thermo Electron 208 Corporation, Model 5012; Petzold and Schönlinner (2004)), providing an independent reference (Fig. S1). The MAAP reported a median concentration of 0.28 μg m^{-3}, approximately 14 % lower than the AE33 median, a difference that has been commonly observed in previous studies (e.g. Salo et al., 2024). An additional intercomparison between the three AE33 instruments was performed using pairwise scatter plots of eBC concentrations. The comparisons show a strong linear agreement between all instrument pairs, with coefficients of determination (R^2) of 0.95 for AE33_2 vs. AE33_1, 0.94 for AE33_3 vs. AE33_1, and 0.95 for AE33_3 vs. AE33_2 (Fig. S2). These results indicate a high level of consistency among the AE33 instruments across the different size fractions measured (PM_1, $PM_{2.5}$, and $PM_{7.2}$), supporting the robustness and comparability of the eBC measurements used in this study. Similarly to the pairwise intercomparison of the AE33 instruments, the comparison between AE33 (AE33_1) and MAAP-derived hourly-averaged eBC concentrations showed a high level of agreement, with a R^2 of 0.96 (Fig. S3).

Absorption across all seven wavelengths was as well evaluated among the AE33 instruments in PM_1. Overall, no significant differences were observed (Fig. S4). Minor variations were noted in the percentile ranges: the 25th and 75th, as well as the 10th and 90th percentiles, were slightly higher at 880 and 950 nm, indicating a small relative increase in absorption at longer wavelengths. These results demonstrate a good agreement among the three AE33 instruments at all measured wavelengths and confirm the reliability of PM_1 eBC measurements during the campaign.

2.2.2 X-ray fluorescence spectroscopy (XRF)

The elemental composition of $PM_{2.5}$ and PM_{10} particles was determined off-line using an energy-dispersive X-ray fluorescence (ED-XRF) spectrometer (model Epsilon4, Malvern Panalytical, Malvern, UK). $PM_{2.5}$ and PM_{10} filter samples (Fluoropore membrane filter, FSLW04700, pore size 3 μm, Merck Life Science, Darmstadt, Germany) were collected for 24 hours using a Lecker sequential sampler, SEQ47/50 (Aurela et al., 2026). In ED-XRF, filter samples are irradiated with a primary X-ray beam. Atoms in the sample are excited and emit secondary (fluorescent) X-rays with characteristic energies specific to each element. By measuring the energy and intensity of these fluorescent X-rays, the concentration of elements such as Al, Si, S, Fe, Cu, Zn, and others can be quantified. The technique is non-destructive and capable of detecting multiple elements simultaneously, covering a wide range from sodium to uranium. In this study, ED-XRF provided detailed information on the

elemental composition of coarse ($PM_{2.5-10}$) and fine ($PM_{2.5}$) particles, allowing the identification of contributions from mineral dust, traffic abrasion (e.g., brake and tyre wear), and other anthropogenic sources. These data were used in combination with AE33 measurements to interpret the sources and properties of measured aerosols. The methodology used to quantify the absolute and relative measurement uncertainties of the ED-XRF elemental concentrations is described in Sect. S3.

2.2.3 Auxiliary instrumentation

Particle number concentrations and size distributions in the aerosol were measured using a Fidas 200 optical particle sizer (Palas, Germany). The Fidas instrument determines particle sizes based on light scattering: aerosol particles pass through a laser beam, and the intensity of scattered light is measured at defined angles. The signal is converted into particle size using Mie scattering theory, allowing simultaneous classification into multiple size bins, typically from 0.18 µm to 18 µm in aerodynamic diameter. The instrument provides high-resolution, real-time data on particle number and mass concentrations. In this study, the Fidas data were used to complement the chemical and optical measurements, providing real-time mass concentrations for PM_1, $PM_{2.5}$, and PM_{10} fractions. Basic air quality parameters at the Supersite were continuously monitored using a set of standard instruments: nitrogen oxides (NO_x) were measured with a Horiba APNA-370, ozone (O_3) with a Horiba APOA-370, particle number concentration (PNC; particle size ≥ 10 nm) with an Airmodus A20 CPC, and lung-deposited surface area (LDSA; particle size range ~10-400 nm) of particles with a Pegasor AQ Urban. Street surface state and road water layer was measured with a Vaisala DSC211. In addition, meteorological variables, including ambient air temperature and relative humidity, were recorded directly at the Supersite. Wind speed and direction were measured at roof level in Ilmala, Helsinki, approximately 43 m above ground and about 2 km northwest of the Supersite measurement station.

3 Results and discussion

3.1 Atmospheric Conditions and Pollution Dynamics in the Street Canyon

The atmospheric conditions and major pollutant concentrations during the street-canyon campaign are illustrated in Figure 1. Measurements revealed substantial variability in particulate matter concentrations, reflecting both typical urban emissions and episodic dust events. The campaign hourly mean concentrations were 4.3 µg m^{-3} for PM_1, 7.1 µg m^{-3} for $PM_{2.5}$, and 27.1 µg m^{-3} for PM_{10}, while hourly-averaged PM concentrations ranged from 0.3 and 16.6 µg m^{-3} (PM_1), 0.4 to 35.8 µg m^{-3} ($PM_{2.5}$) and 0.6 to 213 µg m^{-3} (PM_{10}), indicating a strong episodic contribution of coarse particles.

The eBC concentrations in PM_1 were generally low, with an hourly average of 0.48 µg m^{-3}, despite the site being highly influenced by traffic. This suggests a relatively minor PM mass contribution from vehicular exhaust emissions during the campaign period when compared to dust emissions. However, short-term eBC peaks reached 2.76 µg m^{-3}, coinciding with traffic surges and calm weather conditions. Hourly mean PNC averaged 8.27×10^3 particles cm^{-3} per hour, with a maximum of 4.57×10^4 particles cm^{-3}, reflecting episodic particle-rich events likely linked to traffic bursts. Furthermore, concentrations frequently exceeded 20 000 # cm^{-3}, which is the high hourly PNC level defined by the Word Health Organization. Lung-

deposited surface area (LDSA) measurements averaged 10.4 µm² cm⁻³ and peaked at 37.7 µm² cm⁻³. These hourly-averaged values are moderate and do not indicate a particularly high lung-deposited dose compared to more populated and/or polluted urban hotspots (e.g. tunnels or nearby an airport) and regions (Lepistö et al., 2024; Salo et al., 2021).

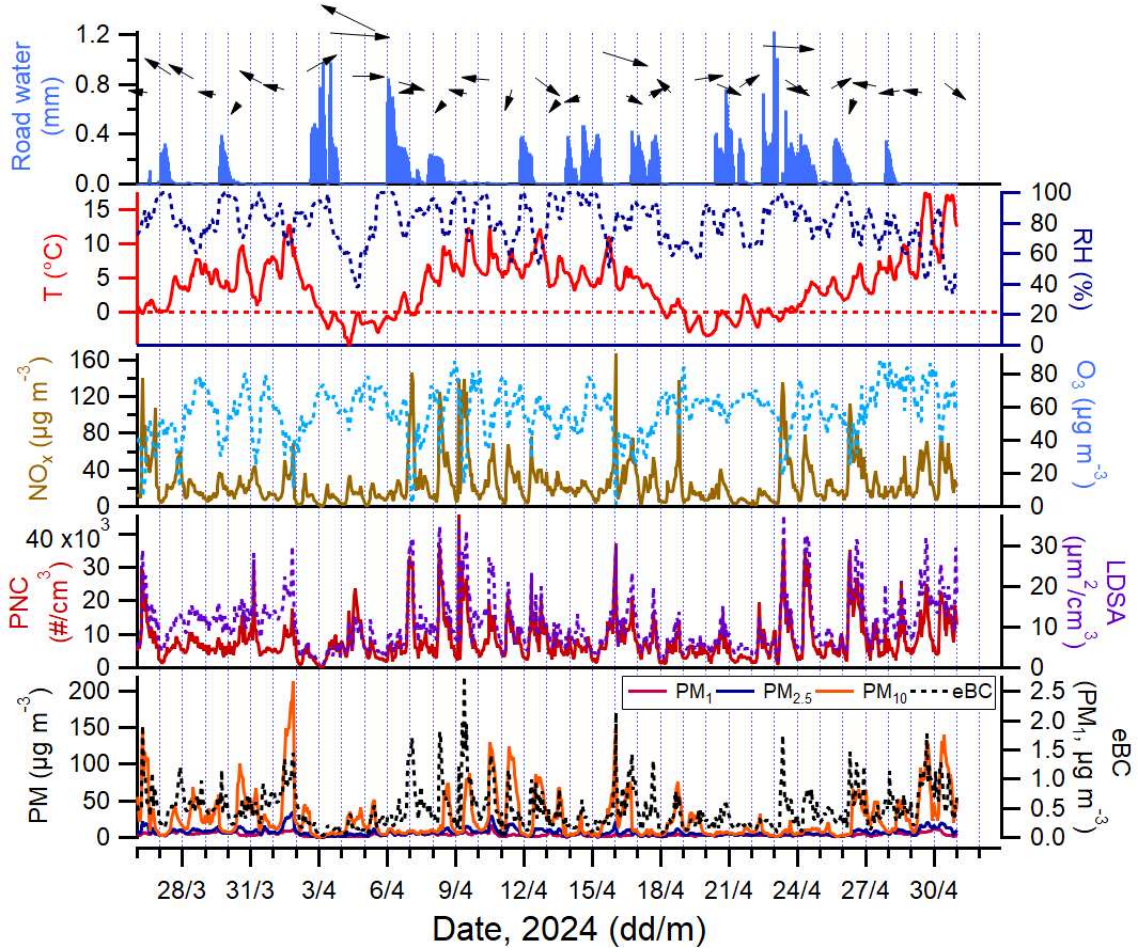

Figure 1: Hourly mean time series of particulate matter mass concentrations (PM_1, $PM_{2.5}$, and PM_{10}), black carbon (eBC in PM_1), particle number concentration (PNC), lung-deposited surface area (LDSA), nitrogen oxides (NO_X), ozone (O_3), air temperature (T), relative humidity (RH), road surface wetness, and daily mean wind direction (wind-speed-weighted, with arrows pointing in the direction of airflow) and speed (semi-quantitatively represented by arrow length) measured during the street-canyon campaign.

Gaseous pollutants reflected expected urban patterns. Nitrogen oxides (NO_X) concentrations displayed clear traffic signatures, peaking during rush hours, with an hourly average of 25.4 µg m⁻³ and maximum of 166.7 µg m⁻³. Ozone concentrations averaged 57.0 µg m⁻³, reaching 87.9 µg m⁻³. These ozone levels are moderate and do not indicate extreme photochemical smog, possibly due to reduction of ozone by NO_X in the street canyon.

Hourly-averaged meteorological conditions were highly variable. Temperature ranged from –4.9 to 17.5 °C, averaging 3.9 °C, while relative humidity ranged from 33.4 % to saturation with an average of 80.4 %. In Nordic countries, a substantial amount of road dust accumulates during winter due to processes such as asphalt wear from studded winter tyres and winter sanding,

and is subsequently released in spring when street surfaces dry out. This seasonal process is consistent with the observed episodic PM_{10} peaks during dry road periods (Figs. 1 and S5). In contrast, wet road conditions, with a maximum water accumulation of 1.2 mm during the campaign, likely suppressed PM_{10} resuspension. Street surfaces were also occasionally covered by snow, ice, or slush (e.g. Aurela et al., 2026), further inhibiting particle resuspension. Accordingly, no elevated PM_{10} concentrations were observed under wet surface conditions (Fig. 1 and S5). Wind direction varied substantially throughout the campaign, although prevailing winds were from the west and east, with maximum wind speeds of 4.64 m s^{-1} and a mean of 1.24 m s^{-1}. These wind patterns likely influenced pollutant dispersion and the episodic dust events observed. Interestingly, PM_{10} concentrations were higher during periods of relatively low wind speed (Fig. S5). This apparent inverse relationship suggests that wind speed alone did not control the observed PM_{10} variability. Instead, elevated concentrations may reflect the combined influence of dry surface conditions, the availability of deposited material for resuspension, traffic-induced mechanical disturbance, and atmospheric stability or reduced dispersion during low-wind conditions. No significant long-range transport events were identified during the campaign.

Overall, the measurements highlight a spring-time street canyon environment dominated by coarse particle events, moderate traffic influence, and highly variable meteorological conditions that may have also influenced PM concentrations. The combination of high PM_{10} peaks, frequent wet surfaces, and variable wind speed underscores the importance of local resuspension in shaping the particulate matter dynamics and properties at this urban site.

3.2 Influence of Sampling Size Cut-Off on Measured Light Absorption and eBC Concentrations

The absorption coefficient of PM was evaluated across the PM_1, $PM_{2.5}$, and $PM_{7.2}$ fractions over the range of AE33 measurement wavelengths (370–950 nm) to assess how the particle-size cut-off influenced measured light absorption. As shown in Fig. 2, light absorption decreased exponentially with increasing wavelength for all PM fractions. Notably, $PM_{2.5}$ exhibited slightly higher absorption than PM_1, and $PM_{7.2}$ consistently showed the highest absorption across all wavelengths. The average PM_1 absorption coefficients ranged from 3.56 to 11.04 Mm^{-1}, while $PM_{2.5}$ and $PM_{7.2}$ ranged from 4.12 to 11.73 Mm^{-1} and 4.93 to 13.28 Mm^{-1}, respectively. Compared to PM_1, $PM_{2.5}$ showed an increase in absorption of approximately 6–16 %, with the largest relative enhancement at 950 nm. More notably, $PM_{7.2}$ absorption increased by 20–39 % relative to the one from PM_1, with the most pronounced rise also occurring at 950 nm. These results indicate that coarse particles can contribute to light absorption, especially at longer wavelengths, highlighting the significant role of larger particles in optical measurements.

To assess whether the enhanced absorption of $PM_{2.5}$ and $PM_{7.2}$ fractions was primarily driven by a higher particle mass, the absorption coefficients were additionally normalized to PM mass to obtain the MAE (Fig. 2). The MAE decreased systematically with increasing wavelength for all size fractions, from 2.70, 1.83, and 0.97 $m^2\ g^{-1}$ at 370 nm to 0.88, 0.65, and 0.35 $m^2\ g^{-1}$ at 950 nm for PM_1, $PM_{2.5}$, and $PM_{7.2}$, respectively. Thus, although $PM_{7.2}$ exhibited the highest absolute absorption, its absorption per unit mass was substantially lower than that of the finer fractions. This indicates that the 20–39% enhancement

in $PM_{7.2}$ absorption relative to PM_1 is largely associated with the greater mass of particles present in the coarse fraction rather than a higher intrinsic absorption efficiency.

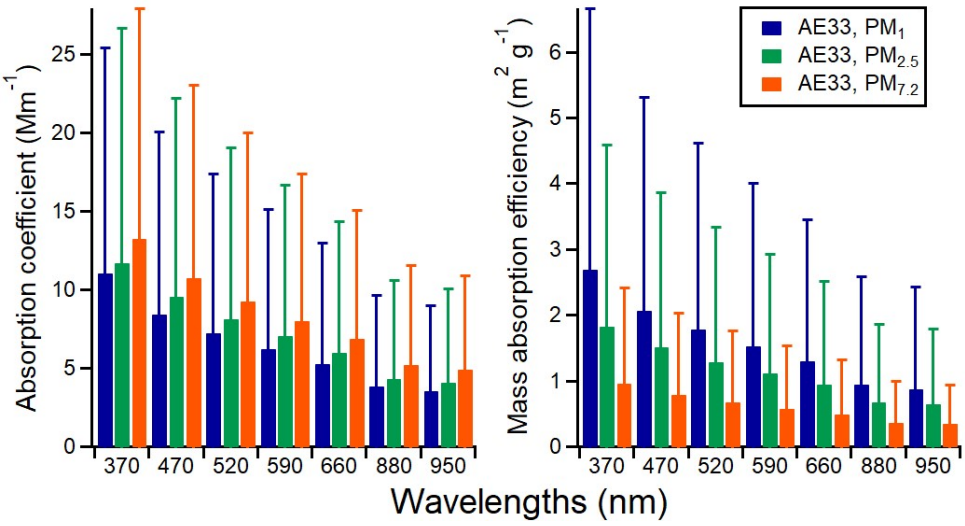

Figure 2: Campaign-averaged wavelength-dependent absorption coefficients (left plot) and mass absorption efficiency (right plot) of particulate matter (PM) for PM_1, $PM_{2.5}$, and $PM_{7.2}$ fractions, measured with the AE33 aethalometer across 370–950 nm. Error bars indicate ±1 standard deviations.

The effect of sampling different particulate matter size fractions on the Absorption Ångström Exponent (AAE) was also evaluated. The AAE time series for the campaign is shown in Fig. S6, and multiple wavelength pairs were used to capture spectral dependence, specifically $AAE_{370/470}$, $AAE_{470/520}$, $AAE_{370/950}$, and $AAE_{470/950}$. The shorter wavelength pairs (370–470 and 470–520) are particularly sensitive to enhanced absorption by brown carbon (BrC) and other species that preferentially absorb at lower wavelengths, whereas combinations including 950 nm (370–950 and 470–950) are more commonly used to represent the overall AAE and characterize bulk aerosol absorption (e.g. Helin et al., 2021). As illustrated in Fig. 3, AAE varied substantially across the different PM fractions, indicating that particle size influences the wavelength dependence of light absorption. For $AAE_{370/470}$, values decreased from 1.12 for PM_1 to 0.77 for $PM_{2.5}$ and 0.86 for $PM_{7.2}$, suggesting a relative weakening of short-wavelength absorption with increasing particle size.

Among the wavelength pairs, $AAE_{370/470}$ also exhibited the largest temporal variability, including several nighttime low spikes in the $PM_{2.5}$ fraction (Fig. S6). A particularly noticeable low spike occurred between 2 and 3 April, when $AAE_{370/470}$ reached approximately -5 around 01:30 (Fig. S6). Such anomalously low values may be associated with very low absorption coefficients (Fig. S7), where increased uncertainty in the optical measurements can lead to unstable or unrealistic AAE values, particularly for short-wavelength pairs. In contrast, $AAE_{370/950}$ (1.21, 1.10, and 1.06 for PM_1, $PM_{2.5}$, and $PM_{7.2}$, respectively) and $AAE_{470/950}$ (1.24, 1.21, and 1.13) showed smaller differences between size fractions, indicating that the inclusion of near-infrared wavelengths, where BC absorption becomes more dominant, reduces sensitivity to particle size effects. For $AAE_{470/520}$, values were consistently higher overall (1.50–1.61), with $PM_{2.5}$ exhibiting the largest value, pointing to enhanced spectral

curvature in the mid-visible range. This wavelength dependence could be consistent with absorption by chromophores in the 450–600 nm range (e.g. nitroaromatic compounds) (e.g. Lin et al., 2017; Xie et al., 2017). However, chromophores were not chemically measured and identified in detail in this study across different fractions, and further chemical analysis would be required to assess their potential relative contribution to aerosol absorption in these fractions.

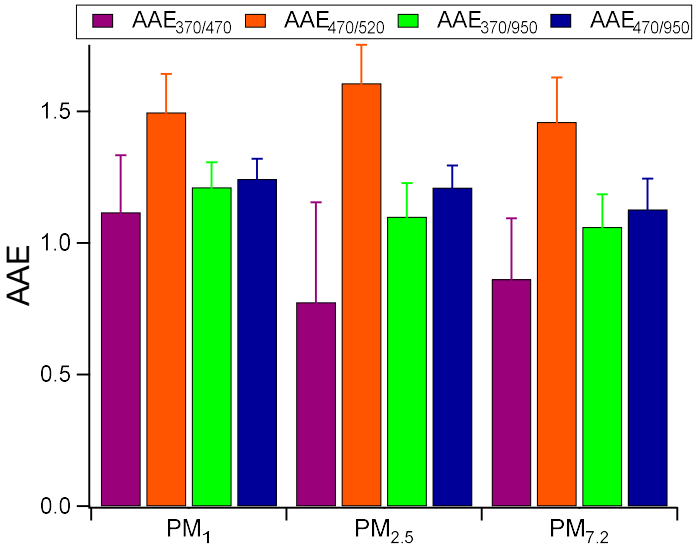

Figure 3: Campaign-averaged Absorption Ångström Exponent (AAE) values for different wavelength pairs (370/470, 470/520, 370/950, and 470/950 nm) across PM_1, $PM_{2.5}$, and $PM_{7.2}$ size fractions. Error bars indicate ±1 standard deviations.

AAE for PM_1 slightly above unity are commonly reported in traffic-influenced environments where black carbon absorption typically dominates, particularly when AAE is derived using longer wavelength pairs such as 470/950 nm (e.g. Helin et al., 2021). In contrast, the slightly lower AAE values observed for coarse fractions imply a shift toward more spectrally neutral absorbers as particles grow, which is expected considering the dominance of eBC regarding light absorption. The results are consistent with previous modeling studies (e.g. Virkkula, 2021), which show that $AAE_{470/950}$ depends on both particle size and coating thickness. This highlights that differences in the sampled particle population can affect the interpretation of aerosol optical properties and should be considered when comparing measurements obtained using different PM size cut-offs.

The interpretation of AAE becomes particularly challenging for coarse-mode aerosols because the classical framework linking spectrally neutral absorption primarily to BC and enhanced short-wavelength absorption to BrC does not necessarily account for the full range of absorbing components present in larger particles. As mentioned previously, coarse particles may contain light-absorbing materials such as iron oxides associated with mineral dust as well as carbonaceous components originating from non-exhaust traffic emissions, including tyre and brake wear (e.g. Apicella et al., 2026; Di Biagio et al., 2019; Khardi, 2024). These components may exhibit their own wavelength dependence, meaning that changes in AAE across PM size fractions cannot be uniquely attributed to changes in the relative contributions of BC and BrC. Consequently, AAE should be interpreted primarily as an optical descriptor rather than a direct source tracer, particularly when the sampled size range extends into the coarse mode. This limitation is also relevant for AAE-based biomass-burning source apportionment. The estimation

of BB% from AE33 measurements commonly relies on the assumption that enhanced short-wavelength absorption relative to BC is primarily associated with BrC from biomass-burning aerosol. When coarse particles contribute substantially to absorption, however, non-BC absorbing components such as mineral dust and non-exhaust carbonaceous materials may invalidate this assumption, resulting in uncertain or potentially biased BB% estimates. Thus, the observed differences in AAE between PM fractions should be considered when applying AAE-based source-apportionment approaches, particularly for size fractions extending beyond $PM_{2.5}$.

To further investigate the relationship between size fractions, correlations between the absorption coefficients of $PM_{2.5}$ versus PM_1 (bottom panels) and $PM_{7.2}$ versus PM_1 (top panels) were examined for three representative wavelengths in Fig. 4 (370 nm (left), 520 nm (middle), and 880 nm (right)). The correlation between $PM_{2.5}$ and PM_1 was high, with coefficient of determination (R^2) values ranging from 0.98 to 0.99 across all wavelengths, indicating that the submicron particles largely governed absorption in fine fraction. In contrast, correlations between $PM_{7.2}$ and PM_1 were slightly weaker, with R^2 values between 0.86 and 0.89, reflecting the additional variability introduced by the coarse fraction. Examination of the scatter plots suggests that elevated PM_{10} mass concentrations were the main factor driving the reduced correlation, as high values consistently lie above the 1:1 slope line, indicating that coarse particles can increase absorption beyond that expected from PM_1 alone. These results reinforce the fact that coarse particles in $PM_{7.2}$ and above can modulate absorption, including the wavelengths where absorption is often assumed to be only caused by BC particles.

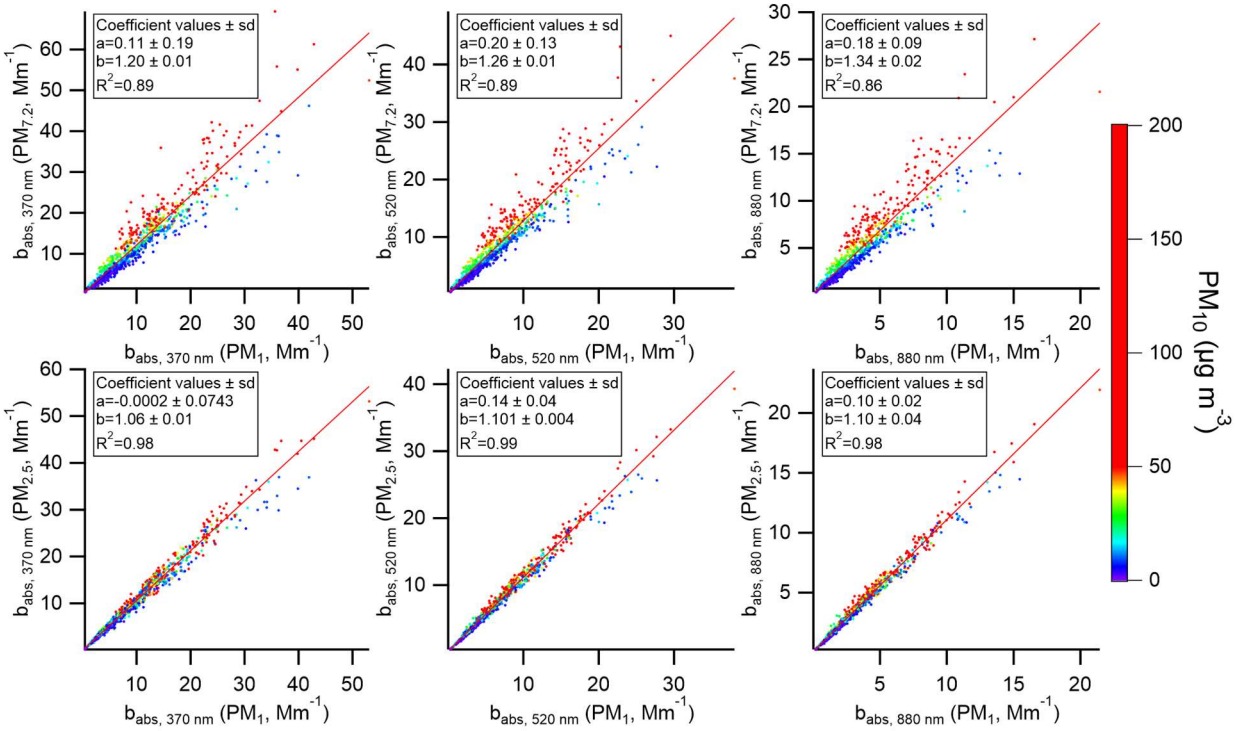

Figure 4: Correlation between hourly-averaged absorption coefficients of different PM size fractions at three representative wavelengths (top panels: $PM_{7.2}$ versus PM_1; bottom panels: $PM_{2.5}$ versus PM_1; left: 370 nm, middle: 520 nm, right: 880 nm).

Due to the differences in light absorption across size fractions, the corresponding AE33-derived eBC concentrations were evaluated across the PM_1, $PM_{2.5}$, and $PM_{7.2}$ fractions (Fig. S8). The campaign-averaged eBC concentrations were 0.49 μg m^{-3} in PM_1, 0.56 μg m^{-3} in $PM_{2.5}$, and 0.68 μg m^{-3} in $PM_{7.2}$. Compared to hourly averaged eBC concentrations in PM_1, those in $PM_{2.5}$ were on average 14 ± 10 % higher, while $PM_{7.2}$ showed a larger increase of 41 ± 36 % over the campaign period. These results highlight the influence of the inlet cut-off size on the measured eBC. However, the observed increase should not necessarily be interpreted as an equivalent increase in actual black carbon mass, as coarse non-BC absorbing particles can contribute to the measured attenuation. These results highlight the influence of the inlet cut-off size on A33-derived eBC concentrations. Using a PM_1 and/or $PM_{2.5}$ inlet, as e.g. in the Helsinki Region Environmental Services Authority (HSY) network (e.g. Barreira et al., 2021; Saarikoski et al., 2023), targets light-absorbing carbonaceous aerosol in the submicron and fine fractions, which minimizes interference from coarse-mode particles such as road dust. This is well suited for tracking long-term trends in combustion-related black carbon emissions (e.g. from traffic and residential wood burning), where the objective is to capture changes in soot rather than mechanically generated dust. PM_1 light absorption measurements are also directly comparable with submicron aerosol chemical composition measurements from instruments such as the ACSM (Aerosol Chemical Speciation Monitor). In contrast, ACTRIS prescribes that the PM_{10} size fraction must be used, except in situations where a whole-air inlet is required, leading to higher measured eBC (ACTRIS, 2024). Consequently, measurements from different networks are not directly comparable unless the size fraction is consistent. This issue becomes particularly relevant under the new EU Air Quality Directive (2024/2881), which requires Member States to monitor black carbon at designated supersites but does not specify a particle-size cut-off (European Union, 2024). Until harmonized guidance emerges, differences in sampling fraction will remain a major source of variability in eBC datasets, underscoring the need for explicit reporting of the applied size cut-off when comparing or interpreting black carbon measurements. In particular, for larger particle fractions, eBC may be overestimated when non-BC absorbing components, such as mineral dust or brown carbon, contribute substantially to the measured absorption, because the absorption is converted to eBC using a BC-specific mass absorption cross-section.

Recent studies have also examined how light absorption varies with aerosol size, composition, and sampling fraction. For instance, the work by Savadkoohi et al. (2024) in RI-URBANS project emphasized that optical measurements of light absorption derive from measured absorption coefficients and require use of a mass-absorption cross-section (MAC), which itself depends on particle size distribution and composition. Moreover, study by Mishra et al. (2025) comparing optical absorption and isotopic composition in PM_{10} and $PM_{2.5}$ from different emission sources found distinct absorption characteristics depending on particle size and source type, suggesting that coarse PM may contribute significantly to total absorption under certain conditions. Similarly, a recent investigation focusing on aerosol extracts, comparing PM_{10} and $PM_{2.5}$, highlighted that absorption of organic matter from coarse PM can differ notably from fine PM, due to differences in chemical composition and surface reactions (Cui et al., 2025). This supports the notion that size fractions larger than PM_1 cannot simply be ignored when interpreting absorption-based measurements. However, many earlier studies, particularly in pollution-dominated or dust-plume environments, have focused on fine-mode particles (e.g., BC in $PM_{2.5}$ or PM_1) as the primary

absorbers, while coarse particles (e.g., mineral dust) are often considered mainly scattering components (Moteki, 2023; e.g. Pu et al., 2015).

Nonetheless, selecting only larger particle size fractions may introduce additional uncertainty in AE33-derived eBC, because absorption in larger particles can originate from both true light-absorbing material (e.g., internally mixed black carbon) and non-BC absorbing components such as mineral dust and other light-absorbing material. In addition, the fixed multiple-scattering correction applied by the AE33 (C_{ref}=1.39) is calibrated for submicron BC-rich particles, assuming an optical behavior typical of fine combustion particles. Therefore, this correction factor may not fully account for the optical properties of the coarse fraction, which is characterized by stronger scattering and a greater contribution from non-BC absorbing components. Consequently, increased eBC in larger size fractions does not necessarily indicate an increase in actual black carbon mass. A further limitation concerns the use of the FIDAS optical spectrometer for coarse-mode characterization since its optical response is sensitive to scattering by large particles and to assumptions regarding particle refractive index and shape, which may distort or overestimate dust-related PM peaks (e.g. Meyer et al., 2026; Yus-Díez et al., 2025). Taken together, these considerations highlight the importance of selecting the appropriate PM size fraction when quantifying light absorption and light-absorption components such as eBC, as well as when interpreting potential source contributions.

3.3 Size-Resolved Contributions of Fine and Coarse Aerosol Fractions to Light Absorption

To better understand the contributions of different particle-size fractions to light absorption and their relative importance across the aerosol size spectrum, the absorption coefficients measured by the AE33 at seven wavelengths (370–950 nm) were partitioned into the PM_1, $PM_{1\text{-}2.5}$, and $PM_{2.5\text{-}7.2}$ fractions (Fig. 5). The complete time series of these size-resolved absorption coefficients, along with the corresponding PM_1, $PM_{2.5}$, and PM_{10} mass concentrations for comparison, is shown in Fig. S7. This size-differentiated approach allows the contributions of submicron, 1–2.5 µm, and 2.5–7.2 µm particles to wavelength-dependent aerosol light absorption to be evaluated separately.

Across all wavelengths, PM_1 clearly dominated total absorption (values reported in Sect. 3.2). The monotonic decrease in absorption with wavelength reflects the expected spectral dependence of BC-rich aerosols, although additional enhancement from light-absorbing organics may occur at shorter wavelengths (e.g. Barreira et al., 2024). The $PM_{1\text{-}2.5}$ fraction contributed substantially less to total absorption, with campaign-averaged coefficients ranging from 0.48 Mm^{-1} at 880 nm to 1.13 Mm^{-1} at 470 nm. Furthermore, it showed a relatively weak wavelength dependence compared with PM_1, indicating a lower abundance of strongly absorbing carbonaceous material. Nevertheless, the enhancement in light absorption from 370 to 470 nm in the $PM_{1\text{-}2.5}$ fraction suggests the presence of additional light-absorbing components beyond those typically associated with PM_1 particles. The $PM_{2.5\text{-}7.2}$ fraction also showed modest absorption, ranging from 0.85 Mm^{-1} at 950 nm to 1.66 Mm^{-1} at 370 nm. This does not necessarily imply that $PM_{2.5\text{-}7.2}$ was intrinsically more absorbing than $PM_{1\text{-}2.5}$, because the absorption coefficient depends on both particle mass and mass-specific absorption efficiency. The observed coarse-mode absorption may therefore reflect its larger mass loading together with contributions from light-absorbing components potentially associated with mineral dust and mechanically generated particles, including brake and rail wear (e.g. Ansari and Ramachandran, 2025; Chan et al.,

2002; Ito et al., 2018; Liu et al., 2022b). Without size-resolved compositional information, however, these source contributions cannot be assigned unambiguously.

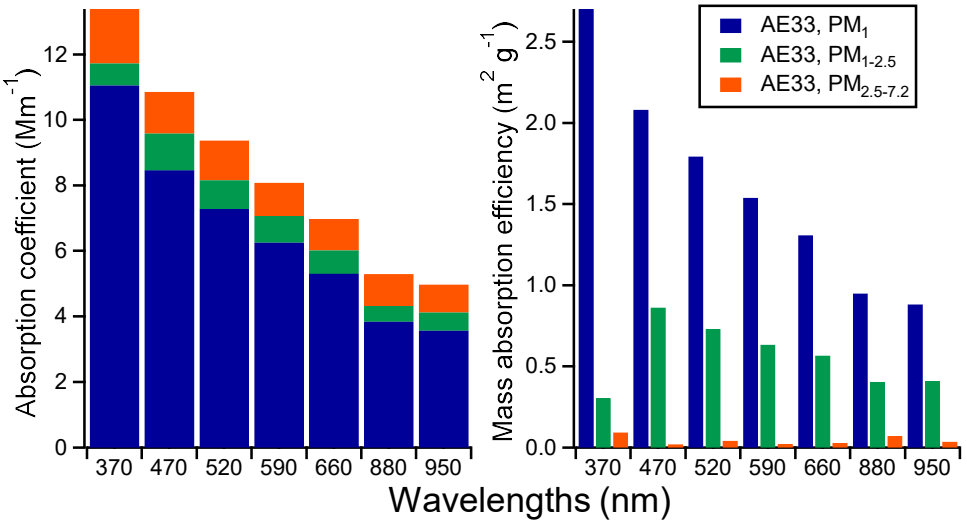

Figure 5: Wavelength-dependent absorption coefficient (left plot) and mass absorption efficiency (right plot) for different PM size fractions (PM_1, $PM_{1-2.5}$, and $PM_{2.5-7.2}$). In the left plot, PM_1 is shown at the bottom, the $PM_{1-2.5}$ fraction in the middle, and the $PM_{2.5-7.2}$ fraction at the top, illustrating the contribution of each size range to total light absorption across the AE33 measurement wavelengths (370-950 nm).

The size-resolved MAE results further clarified this distinction between absorption contribution and absorption efficiency (Fig. 5). PM_1 exhibited by far the highest MAE across the investigated wavelength range, demonstrating that submicron particles were the most efficient light absorbers per unit mass. The 1–2.5 µm fraction nevertheless exhibited appreciable MAEs, particularly from 470 to 950 nm where values decreased from 0.86 to 0.41 $m^2\ g^{-1}$, indicating the presence of light-absorbing material within the larger fine-particle fraction. In contrast, the MAEs of the 2.5–7.2 µm fraction were substantially lower (0.03 to 0.09 $m^2\ g^{-1}$). Because PM_{10} rather than $PM_{7.2}$ mass concentrations were available, these values were normalized by the $PM_{2.5-10}$ mass concentration and therefore represent an approximation of the absorption efficiency of the coarse fraction. Their low values nevertheless indicate that larger particles were much less efficient light absorbers on a mass basis than PM_1. Their measurable contribution to the absorption coefficient therefore appears to arise, at least partly, from their larger particle mass rather than from high mass-specific absorption efficiency.

Overall, PM_1 accounted for the dominant fraction of light absorption across all wavelengths, whereas the $PM_{1-2.5}$ and $PM_{2.5-7.2}$ fractions made smaller but measurable contributions. The $PM_{2.5-7.2}$ fraction contributed more to the absorption coefficient than $PM_{1-2.5}$ at several wavelengths, despite having a much lower MAE, highlighting the importance of distinguishing between a size fraction's absolute contribution to light absorption and its absorption efficiency per unit mass. These results demonstrate that light absorption was primarily associated with submicron aerosol, while particles larger than 1 µm provided additional, although substantially smaller, contributions to the overall absorption budget.

The effect of using upper particle-size cut-offs ($PM_{2.5}$ and $PM_{7.2}$) on eBC concentrations was also evaluated. The campaign-averaged values showed a strong size dependence, with PM_1 clearly dominating (Fig. S9). The $PM_{1\text{-}2.5}$ and $PM_{2.5\text{-}7.2}$ fractions contributed less to eBC, being 0.06 μg m^{-3} in $PM_{1\text{-}2.5}$, and 0.13 μg m^{-3} in $PM_{2.5\text{-}7.2}$ (Fig. S9), though their relatively higher variability suggests episodic enhancements during dust resuspension events, and/or atmospheric inversion. The additional light absorption associated with the $PM_{1\text{-}2.5}$ and $PM_{2.5\text{-}7.2}$ fractions and the corresponding increase in derived eBC, though smaller than the contribution from PM_1, can influence the total PM absorption and eBC measurements, particularly during dust events. Including these fractions leads to episodic increases in PM absorption and eBC concentrations, which may affect source-specific emission factors or models that assume eBC is confined to the fine mode. Consequently, PM absorption and derived eBC concentrations obtained using different size fractions are not necessarily directly comparable, as larger size fractions may include additional coarse-mode absorbing particles. Accounting for these contributions is therefore important for accurately interpreting urban PM absorption and eBC measurements, evaluating the relative importance of dust versus combustion sources, and incorporating measured absorption parameters into atmospheric models.

Daily variability of absorption coefficients reinforces this interpretation. PM_1 absorption remained relatively stable throughout the day, with only slight increases during morning and evening rush hours (Fig. S10), reflecting the influence of traffic-related particles. This limited diurnal variability likely results from a combination of relatively low traffic emissions and variable meteorological conditions, such as daytime wind and enhanced boundary layer mixing, that can obscure the typical traffic peaks. In contrast, the $PM_{1\text{-}2.5}$ and $PM_{2.5\text{-}7.2}$ fractions showed pronounced daytime enhancements, with absorption peaking around 12:00–13:00. This behavior is consistent with diurnal changes in surface conditions and traffic activity in northern urban environments during springtime road dust seasons, where street surfaces are often moist or frozen in the morning, limiting resuspension, and progressively dry during the day, enabling increased particle release driven primarily by turbulence generated by moving vehicles (e.g., cars, buses, and trams). On the other hand, wind-driven resuspension is generally of minor importance, except under episodic high wind conditions facilitating the entrainment of dust into the $PM_{1\text{-}2.5}$ and $PM_{2.5\text{-}7.2}$ size ranges. Similar diurnal patterns were observed on weekdays (Fig. S11). In contrast, weekends exhibited a distinct PM_1 absorption pattern, likely reflecting changes in traffic intensity and relative contribution of particle sources, while the $PM_{1\text{-}2.5}$ and $PM_{2.5\text{-}7.2}$ fractions retained their midday enhancement, with peak absorption occurring between 12:00 and 15:00, although with lower overall intensity compared with weekdays (Fig. S12). The diurnal profiles of PM_1, $PM_{2.5}$, PM_{10}, and eBC mass concentrations (Fig. S13) support light absorption results: PM_1 closely follows eBC mass, while $PM_{2.5}$ and PM_{10} show stronger daytime increases consistent with dust-dominated patterns.

The gas-phase data further corroborate these findings. The diurnal cycles of NO_X and O_3 (Fig. S14) display clear signatures of traffic emissions, with NO_X exhibiting sharp increases during rush hours, particularly in the morning, and O_3 showing a pronounced decrease between 07:00 and 08:00 due to reduction of ozone by fresh NO from traffic (e.g. Barreira et al., 2021; Liu et al., 2022a). This pattern supports the interpretation that the slight morning enhancement in PM_1 absorption is linked to combustion emissions, while the midday increases in the larger size fractions originate from dust entrainment rather than traffic exhaust sources. Overall, the combined evidence from size-resolved absorption, mass concentrations, and gaseous tracers

indicates that PM_1 absorption in Nordic springtime traffic environments is dominated by BC from combustion; whereas $PM_{1-2.5}$ and $PM_{2.5-7.2}$ absorptions are largely driven by enhanced dust resuspension during daytime conditions favouring road surface drying and increased vehicle-induced turbulence.

3.4 Size-Dependent Light Absorption Under High PM_{10} Dust and Traffic Exhaust Conditions

Light absorption was evaluated across all studied size fractions (PM_1, $PM_{1-2.5}$, and $PM_{2.5-7.2}$) under high PM_{10} dust and high traffic exhaust to assess how contrasting urban pollution regimes modify size-dependent absorption and to distinguish pollution episodes from fresh vehicular emissions and dust (Fig. 6). High PM_{10} dust conditions were defined as $PM_{10} \geq 75^{th}$ percentile (41 μg m^{-3}) with $NO_X \leq 50^{th}$ percentile (17 μg m^{-3}), and high traffic exhaust conditions as $PM_{10} \leq 50^{th}$ percentile (14 μg m^{-3}) with $NO_X \geq 75^{th}$ percentile (36 μg m^{-3}). These conditions occurred in 3 % and 7 % of the total observations for the high PM_{10} dust and high traffic exhaust cases, respectively. This corresponded to $N = 1563$ observations for the high PM_{10} dust category and $N = 3679$ observations for the high-traffic exhaust category. The variability in studied parameters is presented as mean ± SD to account for the variability within each category. The full dataset was also included in the analysis to provide a comprehensive campaign-average perspective.

The distinct aerosol regimes represented by the high PM_{10} dust and high-traffic exhaust categories were further validated using eBC concentrations (Fig. S15) as well as $PM_{2.5}/PM_{10}$ ratios (Fig. S16). Average eBC levels were considerably higher during high-traffic exhaust conditions (0.97 ± 1.38 μg m^{-3}) compared with high PM_{10} dust episodes (0.43 ± 0.50 μg m^{-3}) and the campaign average (0.48 ± 0.71 μg m^{-3}), indicating the stronger influence of fresh combustion emissions in traffic-dominated periods. The $PM_{2.5}/PM_{10}$ ratio also supported this distinction, with high PM_{10} dust conditions showing a coarse-dominated aerosol (19.6 ± 5.2 %), while high-traffic exhaust periods exhibited a fine-particle-dominated regime (62.7 ± 16.3 %); the campaign-average ratio was 46.1 ± 25.6 %. Together, these indicators demonstrate that the classification criteria reliably capture two contrasting aerosol environments, coarse-rich resuspension episodes versus fine-rich traffic emissions, providing a robust basis for interpreting the observed differences in light-absorption across the particle size fractions of this study (PM_1, $PM_{2.5}$, and $PM_{7.2}$).

For the PM_1 fraction, campaign-averaged absorption was the highest under high traffic exhaust conditions, reaching up to 19.2 ± 24.2 Mm^{-1} at the shortest measured wavelength, compared to 10.8 ± 8.1 Mm^{-1} under high PM_{10} dust conditions and 11.0 ± 14.3 Mm^{-1} for the full dataset. This highlights the dominant role of traffic-related ultrafine particles in light absorption. The $PM_{1-2.5}$ fraction contributed less overall but still showed notable variation across conditions: under high PM_{10} dust episodes, campaign-averaged absorption ranged from 0.70 ± 1.15 (880 nm) to 1.59 ± 1.87 (470 nm) Mm^{-1} across the wavelengths, whereas under high traffic exhaust conditions it was near zero or slightly negative at some wavelengths (–0.27 ± 4.2 to 0.95 ± 3.2 Mm^{-1} at 370 and 470 nm, respectively), reflecting the minor role of this fraction in fresh traffic plumes. The campaign-average values for $PM_{1-2.5}$ ranged from 0.48 ± 1.26 (880 nm) to 1.13 ± 2.36 (470 nm) Mm^{-1}, indicating a modest contribution to total absorption.

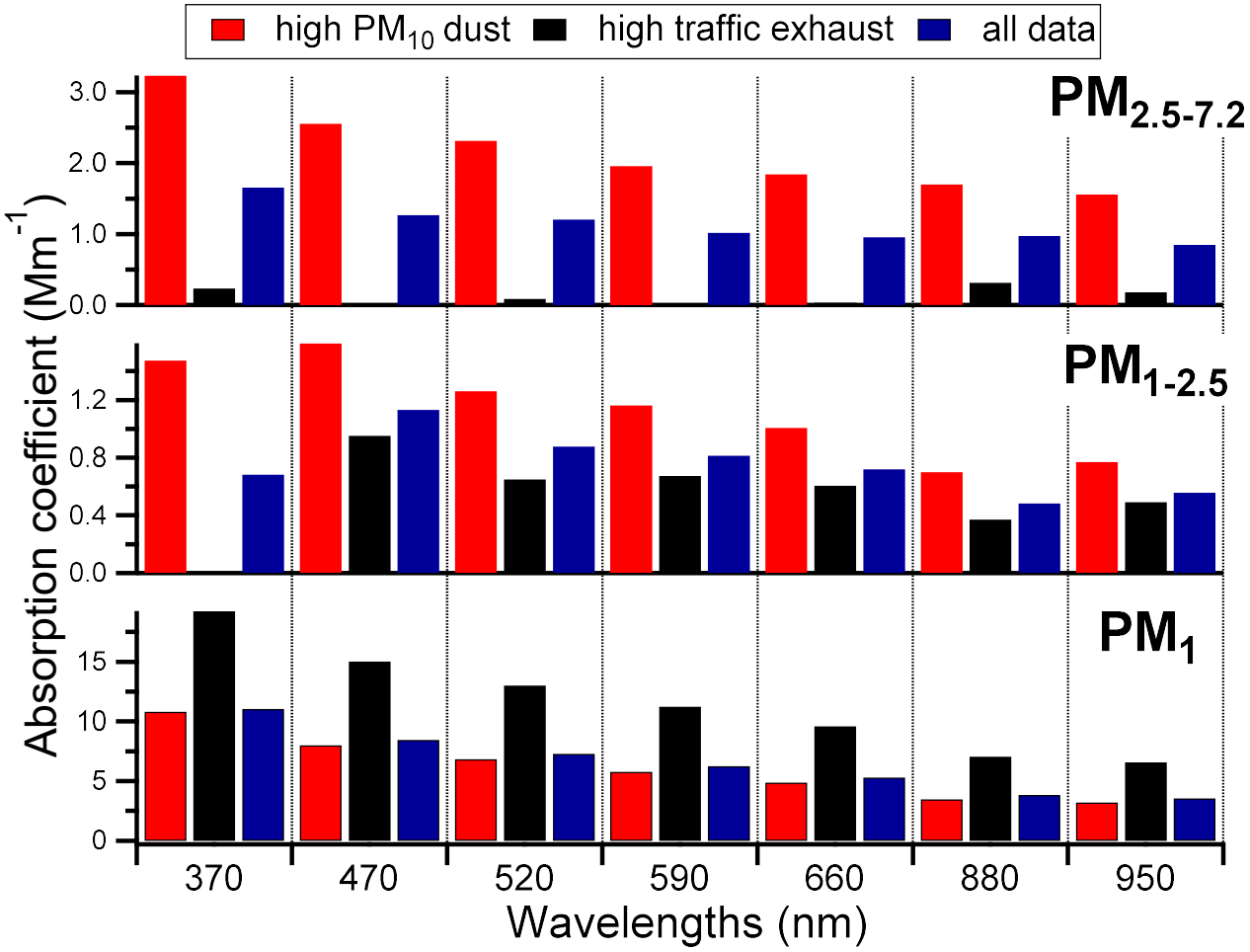

Figure 6: Absorption coefficients as a function of wavelength for different particle size fractions: PM_1 (bottom), $PM_{1\text{-}2.5}$ (middle), and $PM_{2.5\text{-}7.2}$ (top), averaged over the entire campaign under different conditions: high PM_{10} dust (red, $PM_{10} \geq 75^{th}$ percentile and $NO_X \leq 50^{th}$ percentile), high traffic exhaust (black, $PM_{10} \leq 50^{th}$ percentile and $NO_X \geq 75^{th}$ percentile), and all (blue) conditions.

For the $PM_{2.5\text{-}7.2}$ fraction, absorption increased significantly under high PM_{10} dust conditions, with mean values ranging from 1.56 ± 1.69 (950 nm) to 3.23 ± 3.74 (370 nm) Mm^{-1}. Despite the substantial variability within this fraction, the results indicate that coarse particles can make a measurable contribution to light absorption during dust-influenced conditions. In contrast, under high traffic exhaust conditions, absorption by this fraction remained close to zero, ranging from -0.04 ± 9.11 at 470 nm to 0.32 ± 4.70 Mm^{-1}, at 880 nm. The large standard deviations relative to the mean values indicate considerable variability, but the near-zero mean absorption suggests that the $PM_{2.5\text{-}7.2}$ fraction contributes little, on average, to light absorption under fresh traffic-influenced conditions. Across all fractions, absorption generally decreased with increasing wavelength. Interestingly, for the $PM_{2.5\text{-}7.2}$ fraction, a comparison of light absorption with the PMF-derived factors reported by Aurela et al. (2026), based on measurements from the same urban site and sampling period, further highlighted the role of dust in coarse-particle light absorption. Their five-factor PMF solution comprised Dust, Non-exhaust Emissions, Aged Salt, Fresh Salt, and

a mixed Combustion/Secondary Inorganic Aerosol factor. Of these, dust showed the strongest and most consistent positive association with absorption across all wavelengths, with Pearson correlation coefficients (r) ranging from 0.39 to 0.47, whereas correlations with the other factors were generally weak (Table S1). Although these moderate correlations indicate that dust alone does not explain the variability in absorption, the consistent positive association suggests that dust-related coarse particles can contribute appreciably to light absorption during dust-influenced periods.

These findings are consistent with previous studies showing that ultrafine particles from traffic emissions are the dominant contributors to light absorption in urban areas, while larger particles play a secondary but non-negligible role during pollution episodes. For example, BC, that is primarily associated with traffic or incomplete combustion emissions and largely confined to the PM_1 fraction, is widely regarded as the main light-absorbing component in urban aerosols, exhibiting strong absorption across visible wavelengths (Bond and Bergstrom, 2006). In contrast, contributions from coarse-mode particles are often smaller, but under certain pollution episodes, especially those involving dust resuspension or aged aerosols, can enhance absorption or at least influence scattering/absorption balance (e.g. Tohidi et al., 2022).

To further investigate how main aerosol sources influence the wavelength dependence of absorption, the AAE was analysed for PM_1, $PM_{2.5}$, and $PM_{7.2}$ under the previously mentioned pollution regimes (Fig. S17). For comparison purposes, the AAE values for the full campaign dataset are also shown in Fig. S17, although they were previously presented in Sect. 3.2. Under high PM_{10} dust conditions, the AAE exhibited consistently elevated values across all wavelength pairs and size fractions, indicating a pronounced wavelength dependence of absorption. For $AAE_{370/470}$, values were 1.23 ± 0.23, 1.07 ± 0.30, and 1.03 ± 0.25 for PM_1, $PM_{2.5}$, and $PM_{7.2}$, respectively. Similarly, $AAE_{370/950}$ (1.30 ± 0.12, 1.22 ± 0.14, and 1.12 ± 0.13) and $AAE_{470/950}$ (1.32 ± 0.09, 1.28 ± 0.10, and 1.16 ± 0.10) decreased slightly with increasing particle size, suggesting a modest reduction in spectral dependence in the coarse fraction when near-infrared wavelengths are included. $AAE_{470/520}$ displayed the highest values overall (1.60 ± 0.18, 1.71 ± 0.18, and 1.59 ± 0.16), indicating strong spectral curvature in the mid-visible range during dust-dominated episodes.

In contrast, high traffic exhaust conditions were characterized by generally lower AAE values, particularly for the $PM_{7.2}$ fraction, indicating a weaker wavelength dependence of light absorption. For $AAE_{370/470}$, values were 1.04 ± 0.17, 0.73 ± 0.13, and 0.78 ± 0.22 for PM_1, $PM_{2.5}$, and $PM_{7.2}$, respectively. $AAE_{370/950}$ remained close to unity across all size fractions (1.13 ± 0.08, 1.04 ± 0.06, and 1.03 ± 0.10), consistent with a black carbon–dominated absorption regime typical of fresh combustion emissions. The $AAE_{470/950}$ (1.17 ± 0.06, 1.15 ± 0.07, and 1.12 ± 0.07) was slightly higher and more invariant across particle sizes, likely due to the increased contribution of near-infrared absorption, where black carbon exhibits relatively spectrally flat behavior and reduced sensitivity to e.g. particle coating or mixing state effects. Although $AAE_{470/520}$ was somewhat higher (1.40 ± 0.09, 1.53 ± 0.11, and 1.44 ± 0.11), this enhancement is restricted to the mid-visible range and does not indicate strong overall spectral dependence of absorption.

A direct comparison between the two regimes highlights clear differences in aerosol optical behavior. Dust-dominated conditions consistently produce higher AAE values across all wavelength pairs, reflecting stronger wavelength-dependent absorption associated with mineral dust and mixed aerosol populations. In contrast, traffic exhaust conditions are characterized

by AAE values closer to unity, particularly for $PM_{7.2}$ and at longer wavelength pairs ($AAE_{370/950}$ and $AAE_{470/950}$), consistent with black carbon–dominated and more spectrally neutral absorption. This difference affects the estimation of several key parameters. For instance, $AAE_{470/950}$ values, together with assumed AAE values for fossil fuel and biomass burning emissions, are commonly used to estimate the relative contribution of biomass burning aerosol (see Eq. (3)), expressed as BB% (e.g. Helin et al., 2018). Therefore, BB% is highly influenced by the spectral dependence of light absorption, which makes the derived source apportionment highly sensitive to changes in spectral slope. In this study, the corresponding campaign-averaged BB% values were 25 ± 14 %, 20 ± 15 %, and 6 ± 20 %, respectively (Fig. S18). The sequential decrease in BB% from PM_1 to $PM_{2.5}$ and $PM_{7.2}$ was then expected due to the particle-size dependence of the spectral light-absorption properties, although differences in aerosol composition between particle-size fractions were likely the major contributing factor (e.g. Li et al., 2016; Schuster et al., 2006; Utry et al., 2014). Furthermore, negative BB% values were observed, particularly for the fine and coarse PM fractions (Figs. S6 and S18). This indicates that the parameterization typically used for PM_1 is not fully applicable to larger particles, consistent with the observed decrease in $AAE_{470/950}$ with particle size (see Fig. 3). Regarding the distinct aerosol regimes defined in this section, a shift in $AAE_{470/950}$ from the averaged values during traffic-dominated conditions to those during high-dust periods would lead to a substantial increase in the inferred BB% contribution across the studied size fractions (Fig. S18), rising by 233 % for PM_1 (from 12 ± 11 % to 40 ± 18 %), by 256 % for $PM_{2.5}$ (from 9 ± 12 % to 32 ± 18 %), and by 150 % for $PM_{7.2}$ (from 4 ± 13 % to 10 ± 17 %). However, this increase was likely not directly driven by dust itself, as BB% for $PM_{7.2}$ was higher during low-dust and traffic conditions than during high-dust periods (Fig. S18). Overall, the observed results suggest that the variability in BB% was primarily associated with particle-size effects on AAE, whereby lower $AAE_{470/950}$ values for larger size fractions lead to reduced BB% estimates. This interpretation is further supported by the diurnal patterns: dust-related absorption peaks during daytime (Fig. S10) whereas BB% values are consistently higher in the evening (Fig. S19), indicating a decoupling between dust-driven absorption and the inferred biomass burning percentage.

In addition, AAE is often used to estimate BrC absorption under the assumption of AAE = 1 (e.g. Barreira et al., 2024; Zhang et al., 2019). Therefore, differences in aerosol composition between size fractions that alter AAE can influence BrC-related estimates, since variations in AAE directly propagate into the assumed partitioning between black carbon and non-BC absorbing components.

Overall, these results demonstrate that aerosol source type strongly controls the spectral dependence of light absorption. Dust episodes enhance wavelength-dependent absorption across the visible spectrum, while traffic exhaust emissions lead to more spectrally neutral behavior dominated by black carbon. However, the observed variability across wavelength pairs suggests that caution is needed when interpreting AAE using a limited spectral range, particularly under mixed or traffic-influenced conditions. This underscores the importance of both particle size and emission regime when interpreting AAE and its implications for aerosol composition and radiative effects. These findings should, however, be interpreted in light of the limitations of the available dataset. The statistical analysis of high-PM episodes was limited by the relatively small number of suitable events observed during the measurement period. In particular, additional observations during dust-resuspension events would be valuable for assessing the variability and statistical significance of the coarse-mode contribution to PM absorption

and derived eBC. Future measurement campaigns covering a larger number of such events and a wider range of meteorological and source conditions would therefore provide a more robust basis for evaluating the contribution of coarse-mode aerosol and further strengthen the conclusions of this study.

3.5 Potential Chemical Contributors to Excess Light Absorption in Fine and Coarse particles.

The elemental composition of fine and coarse particles was also examined to assess the potential contribution of elements to the enhanced light absorption observed in both size fractions. While the time series of $PM_{2.5\text{-}7.2}$ absorption and elemental concentrations in $PM_{2.5\text{-}10}$ were analyzed (Fig. 7), the relationship between bulk elemental content and light absorption appeared complex, likely reflecting the effects of particle mixing state, coatings, and chemical interactions. Nevertheless, campaign-averaged concentrations revealed that Si, Fe, and Al were the dominant elements in the coarse fraction, with respective concentrations of 2.6, 1.1, and 0.86 μg m^{-3}. These elements are commonly associated with mineral dust and crustal material (e.g. Remoundaki et al., 2011; Zhang et al., 2018), which can contribute to light absorption, especially when Fe-bearing minerals are present as oxides (e.g., hematite, goethite) or are internally mixed with dark coatings such as black carbon (e.g. Go et al., 2022; Liu et al., 2017; Zhang et al., 2015). Al and Si, while not strongly absorbing in pure form, may participate in forming minerals that can act as substrates for organic or Fe coatings, enhancing overall absorption (e.g. Deboudt et al., 2012).

Overall, the high concentrations of these crustal elements in PM_{10} suggest that coarse-mode mineral particles may be contributing to the observed light absorption, either directly through e.g. Fe-containing mineral phases or indirectly by coating effects. While the individual correlation with absorption is weak, these elements represent a significant potential source of enhanced light absorption in the coarse fraction, providing a basis for further analysis of mineral dust and metal contributions in urban aerosols. In addition to crustal sources, non-exhaust traffic emissions, such as tyre and brake wear, may also contribute to the observed presence of elements in coarse particles (e.g. Lopez et al., 2023). However, the element measurements alone do not allow these sources to be distinguished from mineral or resuspended road dust, particularly for Fe, which can originate from multiple sources and whose chemical form cannot be resolved by XRF. These anthropogenic contributions may therefore represent additional components of the complex mixture of natural and anthropogenic particles influencing the optical properties of coarse particles in urban environments.

In the $PM_{2.5}$ fraction, elemental concentrations were substantially lower than those observed in PM_{10}, indicating a reduced contribution from crustal material (Fig. S20). The dominant elements in $PM_{2.5}$ were Si (0.46 μg m^{-3}), S (0.33 μg m^{-3}), Fe (0.28 μg m^{-3}), Ca (0.16 μg m^{-3}), and Al (0.14 μg m^{-3}). Compared to $PM_{2.5\text{-}10}$, the much smaller mass loadings suggest that mineral dust played a lesser role in fine particles, while secondary species e.g. from combustion-related sources likely became more influential. Although Fe-containing phases were likely present at lower concentrations, they may still contribute disproportionately to light absorption in $PM_{2.5}$ due to their enhanced optical efficiency when internally mixed with black carbon or coated by secondary inorganic or organic material. The presence of sulfur further points to the importance of secondary aerosol formation, which can modify particle mixing state and amplify absorption through lensing and chemical interactions.

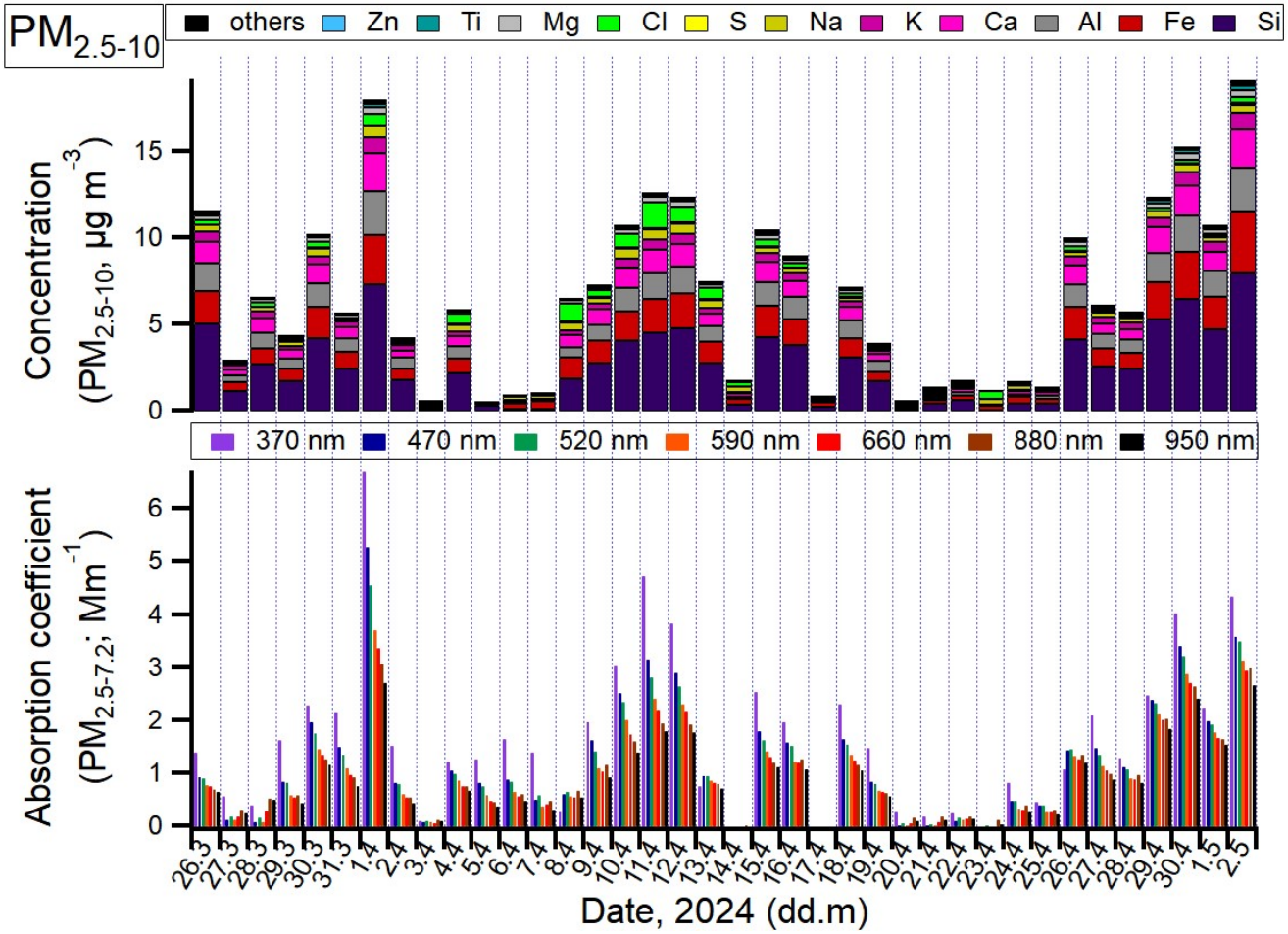

Figure 7: Time series of daily-averaged $PM_{2.5-7.2}$ absorption coefficients, measured by the AE33 aethalometer at seven wavelengths (bottom panel), and $PM_{2.5-10}$ elemental concentrations obtained from XRF analysis of daily filter samples (top panel).

To further investigate the chemical components potentially associated with the observed absorption, source-informed multiple linear regression models were applied to the $PM_{2.5-7.2}$ absorption coefficients at 370, 520, and 660 nm (Tables S2-S4). It should be noted that the absorption measurements represent the $PM_{2.5-7.2}$ fraction, whereas the elemental measurements represent $PM_{2.5-10}$. This size-fraction mismatch should be considered as a limitation when interpreting the relationship between elemental composition and absorption and when extending these results to the full PM_{10} fraction. The models explained a substantial fraction of the observed absorption variability, with R^2 values of 0.751, 0.844, and 0.878 at 370, 520, and 660 nm, respectively (Table S2). Among the selected elemental tracers, Al showed a strong and consistent positive association with absorption at all three wavelengths ($p < 0.001$) (Table S3). The corresponding regression coefficients decreased from 2.07 at 370 nm to 1.31 at 520 nm and 1.06 at 660 nm (Table S3). In contrast, Cu was significant only at 370 nm ($p = 0.031$), while S, Na, and Cl were

not significant predictors at any of the investigated wavelengths (Table S3). However, collinearity diagnostics indicated moderate to high collinearity among some predictors, particularly Na (VIF = 10.19; tolerance = 0.098), which may reduce the stability of individual coefficient estimates (Table S4). Based on the positive regression-derived absorption components, the dust-related contribution represented approximately 67%, 70%, and 80% of the estimated elemental contribution at 370, 520, and 660 nm, respectively. The aged-salt tracer Na accounted for approximately 25%, 23%, and 10% at the same wavelengths, while the contribution associated with S, representing combustion/secondary inorganic aerosol, remained relatively small (approximately 8%, 7%, and 8%).

The strong and consistent association of Al with absorption across all three wavelengths provides additional support for a contribution from mineral dust to the enhanced absorption of the $PM_{2.5-7.2}$ fraction. This is consistent with the PMF analysis, in which the Dust factor showed the strongest and most consistent positive correlation with absorption, while the other source-specific elemental tracers were generally not significant in the regression. However, the regression does not provide a quantitative source apportionment of absorption, as several elemental tracers were themselves correlated, particularly Al with Cu ($r = 0.82$) and Na ($r = 0.74$) (Table S5). These covariations reflect the co-occurrence of different aerosol sources and limit the separation of their individual contributions. Nevertheless, the agreement between the PMF and elemental regression results strengthens the evidence for a dust-related contribution to coarse-particle absorption, while also indicating that the observed enhancement likely reflects a mixture of co-occurring mineral and anthropogenic components that cannot be individually resolved with the available measurements.

The relationship between eBC in $PM_{2.5-7.2}$ and the PMF-derived factors was also examined to assess a potential contribution from carbonaceous material associated with a specific source. eBC was strongly correlated with both Dust ($r = 0.94$) and Non-exhaust Emissions ($r = 0.88$), while correlations with Combustion/Secondary Inorganic Aerosol, Fresh Salt, and Aged Salt were weaker ($r = 0.33$, 0.42, and 0.25, respectively) (Table S6). However, the strong correlation between Dust and Non-exhaust Emissions ($r = 0.89$) indicates a substantial co-variation between these sources (Table S6), preventing their individual contributions to eBC from being distinguished. Thus, results rather indicate that elevated eBC occurred concurrently with periods characterized by both dust and non-exhaust emissions, without demonstrating a distinct contribution from either source.

4 Conclusions

Different size fractions of PM were measured in an urban street canyon during spring, a period characterized by frequent street dust resuspension events and distinct meteorological conditions. Hourly-averaged PM concentrations exhibited substantial variability, with PM_{10} reaching the highest concentrations during episodic dust intrusions, whereas PM_1 and $PM_{2.5}$ remained moderate and eBC concentrations were low, highlighting the dominant influence of episodic dust events. PM_1 particles were predominantly linked to combustion-derived aerosols, reflecting traffic emissions, whereas the $PM_{1-2.5}$ and $PM_{2.5-7.2}$ fractions were strongly influenced by dust events and resuspension, indicating contributions from distinct sources across particle sizes.

Size-resolved light absorption measurements revealed that PM_1 showed a spectral dependence consistent with black carbon, while $PM_{1\text{-}2.5}$ contributed modestly but exhibited enhanced absorption during dust-influenced periods. $PM_{2.5\text{-}7.2}$ showed significant absorption, particularly under high PM_{10} dust conditions, illustrating the likely influence of mineral dust, crustal material, and/or coarse-mode organic aerosols. However, mass-normalized absorption was substantially lower in the coarse fraction than in the finer fractions, indicating that the higher absolute absorption observed for $PM_{2.5\text{-}7.2}$ was largely associated with its greater particle mass. Nevertheless, the MAE of the coarse fraction demonstrates that coarse particles can contribute intrinsically to light absorption and should not be considered optically negligible.

Diurnal patterns indicated that submicron-mode absorption closely followed traffic activity, with morning and evening peaks corresponding to rush hours, while $PM_{1\text{-}2.5}$ and $PM_{2.5\text{-}7.2}$ fractions were influenced by drying dynamics of street surfaces as well as vehicle-driven and wind-driven resuspension. AAE analysis further confirmed strong size- and source-dependent variability, with near-unity values under traffic conditions indicating black carbon dominance, and elevated values during dust episodes reflecting enhanced wavelength-dependent absorption. These results demonstrate that the wavelength dependence of coarse-mode absorption reflects contributions from mineral dust and non-exhaust carbonaceous components, highlighting the complexity of using AAE alone to infer aerosol sources. This variability in AAE can further influence derived aerosol parameters and source apportionment results, including BB% and BrC-related estimates. In particular, the results related to $AAE_{470/950}$ demonstrated that the inclusion of coarse particles can complicate, and potentially compromise, BB% estimation approaches commonly implemented in the AE33-based source apportionment.

Elemental analysis identified Si, Fe, and Al as key constituents of coarse particles, which can absorb light directly in certain chemical forms or serve as substrates for particulate coatings. Non-exhaust traffic emissions, including tyre and brake wear, may have as well introduced metal oxides into coarse fractions, further enhancing absorption. The consistent association of Al with coarse-particle absorption, together with the independent PMF results showing the strongest association between the Dust factor and absorption, provides additional evidence for a dust-related contribution to coarse-mode absorption. However, the covariation among elemental tracers limits the quantitative separation of dust from co-occurring anthropogenic sources, and the regression results should therefore not be interpreted as a quantitative source apportionment. A deeper characterization of chemical composition of coarse particles during non-exhaust events would help confirm the presence of specific compounds and quantify their individual contributions to light absorption.

Overall, the findings highlight the necessity of size-resolved measurements to accurately quantify urban aerosol optical properties, which are controlled by a complex interplay of fine and coarse fractions, their chemical composition and physical properties, and both season-specific and region-specific events. PM_1 dominates absorption associated with black carbon, while $PM_{1\text{-}2.5}$ and $PM_{2.5\text{-}7.2}$ provide smaller but meaningful contributions during dust resuspension episodes. This comprehensive understanding of size-dependent aerosol absorption provides critical insights for air quality management, radiative forcing assessments, and human exposure evaluation in urban environments, particularly in street canyons during periods of enhanced dust activity. At the same time, the interpretation of coarse-mode absorption and derived eBC is subject to additional

uncertainty because the AE33 multiple-scattering correction is calibrated primarily for fine, BC-rich particles and may not fully represent the optical properties of coarse, strongly scattering particles.

Looking forward, non-exhaust emissions are expected to become an increasingly important source of urban particulate matter. In particular, the electrification of vehicles, while reducing tailpipe emissions, may alter non-exhaust PM_{10} contributions: tyre and road wear emissions are likely to persist or potentially increase, for example due to higher vehicle mass, whereas brake wear emissions may decrease due to regenerative braking. Resuspension of road-deposited material, including mineral dust, may also remain an important contributor to coarse-mode PM, particularly under dry conditions. This underscores the importance of studying light absorption in size-resolved particle fractions to better understand the evolving contributions of both fine and coarse aerosols to urban radiative forcing and air quality. Further work is needed to assess the implications of coarse-mode contributions for AAE-based source apportionment, including BB% and BrC estimates particularly given the potential contribution of non-BC absorbing components in the coarse fraction, as well as the applicability of the AE33 multiple-scattering correction to this size fraction. Measurements across a broader range of dust-resuspension conditions would help establish the generality and robustness of the observed coarse-mode contribution to absorption and derived eBC. In parallel, the harmonization of sampling inlets and analytical methods across global measurement networks, while accounting for differences in monitoring objectives, would facilitate more meaningful comparisons across studies and regions. In particular, the use of appropriate size fractions (e.g., PM_1 or $PM_{2.5}$ for urban air quality and BC monitoring, versus PM_{10} for capturing non-exhaust contributions and broader aerosol assessments) would provide more robust and policy-relevant information for mitigating aerosol impacts on climate and health.

Code and data availability

The code and data supporting the findings of this study are available from the corresponding author upon reasonable request.

Author contributions

L.M.F.B. contributed to data curation, formal analysis, investigation, software development, validation, visualization, and writing of the original draft. D.L. contributed to investigation, validation, and writing (review and editing). J.H. contributed to conceptualization, data curation, formal analysis, investigation, methodology, and validation. M.A. contributed to conceptualization, data curation, formal analysis, investigation, methodology, resources, supervision, validation, and writing (review and editing). A.V. contributed to investigation, supervision, validation, and writing (review and editing). J.V.N. contributed to conceptualization, data curation, funding acquisition, investigation, methodology, project administration, resources, supervision, validation, and writing (review and editing). H.E.M. contributed to conceptualization, funding acquisition, investigation, methodology, project administration, resources, supervision, validation, and writing (review and editing). T.R. contributed to conceptualization, funding acquisition, investigation, methodology, project administration,

resources, supervision, validation, and writing (review and editing). H.T. contributed to conceptualization, funding acquisition, methodology, project administration, resources, supervision, and writing (review and editing). S.S. contributed to conceptualization, data curation, formal analysis, funding acquisition, investigation, methodology, project administration, resources, supervision, validation, and writing (review and editing).

Competing interests

At least one of the (co-)authors is a member of the editorial board of Aerosol Research.

Acknowledgements

The authors gratefully acknowledge the institutions that supported this work and the many staff members whose contributions, while not rising to the level of authorship, were essential to the successful completion of this study. The authors acknowledge the use of ChatGPT (OpenAI) for language editing and improvement of the manuscript text.

Financial support

This research was conducted as part of NEX-EL project funded by Business Finland (grant number 8308/31/2022). This work was also supported by the European Union's horizon Europe research and innovation programme under grant agreement No 101096133 (PAREMPI: particle emission prevention and impact: from real-world emissions of traffic to secondary PM of urban air), METECH (Measurement technologies and quantification of exhaust emissions from clean transport solutions) project funded by Business Finland (3971/31/2025, 3973/31/2025) and participating companies, as well as the ACCC Flagship (grant nos. 337552 and 337551) funded by Research Council of Finland.

References

ACTRIS: ACTRIS Standard Procedures for In-Situ Aerosol Sampling, Measurements, and Analyses at ACTRIS Observatories, Version 1.0, Aerosol, Clouds and Trace Gases Research Infrastructure (ACTRIS), https://www.actris-ecac.eu/files/ACTRIS_standard_procedures_for_aerosol_in-situ_measurements.pdf, 2024.

Al-Abadleh, H. A., Motaghedi, F., Mohammed, W., Rana, M. S., Malek, K. A., Rastogi, D., Asa-Awuku, A. A., and Guzman, M. I.: Reactivity of aminophenols in forming nitrogen-containing brown carbon from iron-catalyzed reactions, Commun. Chem., 5, 112, https://doi.org/10.1038/s42004-022-00732-1, 2022.

Al-Abadleh, H. A., Kubicki, J. D., and Meskhidze, N.: A perspective on iron (Fe) in the atmosphere: air quality, climate, and the ocean, Environ. Sci.: Processes Impacts, 25, 151–164, https://doi.org/10.1039/D2EM00176D, 2023.

Ansari, K. and Ramachandran, S.: Enhancing accuracy in identifying absorbing aerosol types and their radiative impacts, npj Clim. Atmos. Sci., 8, 351, https://doi.org/10.1038/s41612-025-01167-w, 2025.

Apicella, B., Catapano, F., Di Iorio, S., Magno, A., and Russo, C.: Non-exhaust emissions: physical and chemical characterization of brake wear particles, Atmos. Res., 336, 108909, https://doi.org/10.1016/j.atmosres.2026.108909, 2026.

Arnott, W. P., Hamasha, K., Moosmüller, H., Sheridan, P. J., and Ogren, J. A.: Towards Aerosol Light-Absorption Measurements with a 7-Wavelength Aethalometer: Evaluation with a Photoacoustic Instrument and 3-Wavelength Nephelometer, Aerosol Sci. Technol., 39, 17–29, https://doi.org/10.1080/027868290901972, 2005.

Aurela, M., Saarnio, K., Niemi, J. V., Turunen, E., Teinilä, K., Kousa, A., Manninen, H. E., Hoivala, J., Vestenius, M., Rönkkö, T., Järvinen, A., Timonen, H., and Saarikoski, S.: Composition and sources of atmospheric trace elements at three urban sites in Helsinki, Finland, Atmos. Environ., 382, 122233, https://doi.org/10.1016/j.atmosenv.2026.122233, 2026.

Banerji, S., Luoma, K., Ylivinkka, I., Ahonen, L., Kerminen, V.-M., and Petäjä, T.: Measurement report: Optical properties of supermicron aerosol particles in a boreal environment, Atmos. Chem. Phys., 25, 16895–16914, https://doi.org/10.5194/acp-25-16895-2025, 2025.

Barreira, L. M. F., Helin, A., Aurela, M., Teinilä, K., Friman, M., Kangas, L., Niemi, J. V., Portin, H., Kousa, A., Pirjola, L., Rönkkö, T., Saarikoski, S., and Timonen, H.: In-depth characterization of submicron particulate matter inter-annual variations at a street canyon site in northern Europe, Atmos. Chem. Phys., 21, 6297–6314, https://doi.org/10.5194/acp-21-6297-2021, 2021.

Barreira, L. M. F., Aurela, M., Saarikoski, S., Li, D., Teinilä, K., Virkkula, A., Niemi, J. V., Manninen, H. E., Pirjola, L., Petäjä, T., Rönkkö, T., and Timonen, H.: Characterizing winter-time brown carbon: Insights into chemical and light-absorption properties in residential and traffic environments, Sci. Total Environ., 955, 177089, https://doi.org/10.1016/j.scitotenv.2024.177089, 2024.

Bond, T. C. and Bergstrom, R. W.: Light Absorption by Carbonaceous Particles: An Investigative Review, Aerosol Sci. Technol., 40, 27–67, https://doi.org/10.1080/02786820500421521, 2006.

Bond, T. C., Anderson, T. L., and Campbell, D.: Calibration and Intercomparison of Filter-Based Measurements of Visible Light Absorption by Aerosols, Aerosol Sci. Technol., 30, 582–600, https://doi.org/10.1080/027868299304435, 1999.

Canagaratna, M. R., Jayne, J. T., Jimenez, J. L., Allan, J. D., Alfarra, M. R., Zhang, Q., Onasch, T. B., Drewnick, F., Coe, H., Middlebrook, A., Delia, A., Williams, L. R., Trimborn, A. M., Northway, M. J., DeCarlo, P. F., Kolb, C. E., Davidovits, P., and Worsnop, D. R.: Chemical and microphysical characterization of ambient aerosols with the aerodyne aerosol mass spectrometer, Mass Spectrom. Rev., 26, 185–222, https://doi.org/10.1002/mas.20115, 2007.

Chan, L. Y., Lau, W. L., Lee, S. C., and Chan, C. Y.: Commuter exposure to particulate matter in public transportation modes in Hong Kong, Atmos. Environ., 36, 3363–3373, https://doi.org/10.1016/S1352-2310(02)00318-7, 2002.

Chen, G., Canonaco, F., Tobler, A., Aas, W., Alastuey, A., Allan, J., Atabakhsh, S., Aurela, M., Baltensperger, U., Bougiatioti, A., De Brito, J. F., Ceburnis, D., Chazeau, B., Chebaicheb, H., Daellenbach, K. R., Ehn, M., El Haddad, I., Eleftheriadis, K., Favez, O., Flentje, H., Font, A., Fossum, K., Freney, E., Gini, M., Green, D. C., Heikkinen, L., Herrmann, H., Kalogridis, A.-C., Keernik, H., Lhotka, R., Lin, C., Lunder, C., Maasikmets, M., Manousakas, M. I., Marchand, N., Marin, C., Marmureanu, L., Mihalopoulos, N., Močnik, G., Nęcki, J., O'Dowd, C., Ovadnevaite, J., Peter, T., Petit, J.-E., Pikridas, M., Matthew Platt, S., Pokorná, P., Poulain, L., Priestman, M., Riffault, V., Rinaldi, M., Różański, K., Schwarz, J., Sciare, J., Simon, L., Skiba, A., Slowik, J. G., Sosedova, Y., Stavroulas, I., Styszko, K., Teinemaa, E., Timonen, H., Tremper, A., Vasilescu, J., Via, M., Vodička, P., Wiedensohler, A., Zografou, O., Cruz Minguillón, M., and Prévôt, A. S. H.: European aerosol phenomenology − 8: Harmonised source apportionment of organic aerosol using 22 Year-long ACSM/AMS datasets, Environ. Int., 166, 107325, https://doi.org/10.1016/j.envint.2022.107325, 2022.

Cui, W., Wang, Z., Feng, W., Qin, C., Liao, H., Wang, Y., and Xie, M.: Evaluating coarse PM composition and sources based on bulk and molecular speciation of PM2.5 and PM10 in Nanjing, East China, J. Environ. Sci., 152, 155–166, https://doi.org/10.1016/j.jes.2024.04.038, 2025.

Deboudt, K., Gloter, A., Mussi, A., and Flament, P.: Red-ox speciation and mixing state of iron in individual African dust particles, J. Geophys. Res. Atmos., 117, https://doi.org/10.1029/2011JD017298, 2012.

Di Biagio, C., Formenti, P., Balkanski, Y., Caponi, L., Cazaunau, M., Pangui, E., Journet, E., Nowak, S., Andreae, M. O., Kandler, K., Saeed, T., Piketh, S., Seibert, D., Williams, E., and Doussin, J.-F.: Complex refractive indices and single-scattering albedo of global dust aerosols in the shortwave spectrum and relationship to size and iron content, Atmos. Chem. Phys., 19, 15503–15531, https://doi.org/10.5194/acp-19-15503-2019, 2019.

Drinovec, L., Močnik, G., Zotter, P., Prévôt, A. S. H., Ruckstuhl, C., Coz, E., Rupakheti, M., Sciare, J., Müller, T., Wiedensohler, A., and Hansen, A. D. A.: The "dual-spot" Aethalometer: an improved measurement of aerosol black carbon with real-time loading compensation, Atmos. Meas. Tech., 8, 1965–1979, https://doi.org/10.5194/amt-8-1965-2015, 2015.

Drinovec, L., Gregorič, A., Zotter, P., Wolf, R., Bruns, E. A., Prévôt, A. S. H., Petit, J.-E., Favez, O., Sciare, J., Arnold, I. J., Chakrabarty, R. K., Moosmüller, H., Filep, A., and Močnik, G.: The filter-loading effect by ambient aerosols in filter absorption photometers depends on the coating of the sampled particles, Atmos. Meas. Tech., 10, 1043–1059, https://doi.org/10.5194/amt-10-1043-2017, 2017.

European Union: Directive (EU) 2024/2881 of the European Parliament and of the Council of 23 October 2024 on ambient air quality and cleaner air for Europe (recast), OJ L, 2024/2881, 20.11.2024, European Union, https://eur-lex.europa.eu/eli/dir/2024/2881/oj/eng, 2024.

Go, S., Lyapustin, A., Schuster, G. L., Choi, M., Ginoux, P., Chin, M., Kalashnikova, O., Dubovik, O., Kim, J., da Silva, A., Holben, B., and Reid, J. S.: Inferring iron-oxide species content in atmospheric mineral dust from DSCOVR EPIC observations, Atmos. Chem. Phys., 22, 1395–1423, https://doi.org/10.5194/acp-22-1395-2022, 2022.

Helin, A., Niemi, J. V., Virkkula, A., Pirjola, L., Teinilä, K., Backman, J., Aurela, M., Saarikoski, S., Rönkkö, T., Asmi, E., and Timonen, H.: Characteristics and source apportionment of black carbon in the Helsinki metropolitan area, Finland, Atmos. Environ., 190, 87–98, https://doi.org/10.1016/j.atmosenv.2018.07.022, 2018.

Helin, A., Virkkula, A., Backman, J., Pirjola, L., Sippula, O., Aakko-Saksa, P., Väätäinen, S., Mylläri, F., Järvinen, A., Bloss, M., Aurela, M., Jakobi, G., Karjalainen, P., Zimmermann, R., Jokiniemi, J., Saarikoski, S., Tissari, J., Rönkkö, T., Niemi, J. V., and Timonen, H.: Variation of Absorption Ångström Exponent in Aerosols From Different Emission Sources, J. Geophys. Res. Atmos., 126, e2020JD034094, https://doi.org/10.1029/2020JD034094, 2021.

Hernández, I. M., González, L. T., Mancilla, Y., Longoria-Rodríguez, F. E., Alfaro, J. M., Pérez-Rodríguez, M., and Mendoza, A.: Assessing black carbon sources with aethalometer data and ambient ΔBC/ΔCO ratios analysis, Sci Rep, 15, 35716, https://doi.org/10.1038/s41598-025-19646-8, 2025.

Ito, A., Lin, G., and Penner, J. E.: Radiative forcing by light-absorbing aerosols of pyrogenetic iron oxides, Sci. Rep., 8, 7347, https://doi.org/10.1038/s41598-018-25756-3, 2018.

Jayne, J. T., Leard, D. C., Zhang, X., Davitovits, P., Smith, K. A., Kolb, C. E., and Worsnop, D. R.: Development of an Aerosol Mass Spectrometer for Size and Composition Analysis of Submicron Particles, Aerosol Sci. Technol., 33, 49–70, https://doi.org/10.1080/027868200410840, 2000.

Kahnert, M. and Kanngießer, F.: Modelling optical properties of atmospheric black carbon aerosols, J. Quant. Spectrosc. Radiat. Transfer, 244, 106849, https://doi.org/10.1016/j.jqsrt.2020.106849, 2020.

Kakavas, S. and Pandis, S. N.: Effects of urban dust emissions on fine and coarse PM levels and composition, Atmos. Environ., 246, 118006, https://doi.org/10.1016/j.atmosenv.2020.118006, 2021.

Khardi, S.: Emission Factors of Tyre Wear Particles Emitted by Light Road Vehicles in Real Driving Conditions: A New Challenge for Clean Road Transport to Improve Urban Air Quality, Atmosphere, 15, 665, https://doi.org/10.3390/atmos15060665, 2024.

Kozawa, K. H., Park, S. S., Mara, S. L., and Herner, J. D.: Verifying Emission Reductions from Heavy-Duty Diesel Trucks Operating on Southern California Freeways, Environ. Sci. Technol., 48, 1475–1483, https://doi.org/10.1021/es4044177, 2014.

Kupiainen, K., Ritola, R., Stojiljkovic, A., Pirjola, L., Malinen, A., and Niemi, J.: Contribution of mineral dust sources to street side ambient and suspension PM10 samples, Atmos. Environ., 147, 178–189, https://doi.org/10.1016/j.atmosenv.2016.09.059, 2016.

Lee, M. G., Ryu, H., Hyun, M., Chung, W., Hong, J., Kim, H., Kwon, J.-T., Lee, J., and Kim, Y.: Mass flow analysis of tire-wear particles, including carbon black, and implications for road dust management, Atmos. Environ., 351, 121184, https://doi.org/10.1016/j.atmosenv.2025.121184, 2025.

Lepistö, T., Lintusaari, H., Salo, L., Silvonen, V., Barreira, L. M. F., Hoivala, J., Markkula, L., Niemi, J. V., Ondracek, J., Teinilä, K., Manninen, H. E., Saarikoski, S., Timonen, H., Dal Maso, M., and Rönkkö, T.: Comparison of size distribution and electrical particle sensor measurement methods for particle lung deposited surface area ($LDSA^{al}$) in ambient measurements with varying conditions, Aerosol Res., 2, 271–289, https://doi.org/10.5194/ar-2-271-2024, 2024.

Li, J., Liu, C., Yin, Y., and Kumar, K. R.: Numerical investigation on the Ångström exponent of black carbon aerosol, J. Geophys. Res. Atmos., 121, 3506–3518, https://doi.org/10.1002/2015JD024718, 2016.

Lin, P., Bluvshtein, N., Rudich, Y., Nizkorodov, S. A., Laskin, J., and Laskin, A.: Molecular Chemistry of Atmospheric Brown Carbon Inferred from a Nationwide Biomass Burning Event, Environ. Sci. Technol., 51, 11561–11570, https://doi.org/10.1021/acs.est.7b02276, 2017.

Liu, C., Chung, C. E., Yin, Y., and Schnaiter, M.: The absorption Ångström exponent of black carbon: from numerical aspects, Atmos. Chem. Phys., 18, 6259–6273, https://doi.org/10.5194/acp-18-6259-2018, 2018.

Liu, D., Whitehead, J., Alfarra, M. R., Reyes-Villegas, E., Spracklen, D. V., Reddington, C. L., Kong, S., Williams, P. I., Ting, Y.-C., Haslett, S., Taylor, J. W., Flynn, M. J., Morgan, W. T., McFiggans, G., Coe, H., and Allan, J. D.: Black-carbon absorption enhancement in the atmosphere determined by particle mixing state, Nat. Geosci., 10, 184–188, https://doi.org/10.1038/ngeo2901, 2017.

Liu, T., Sun, J., Liu, B., Li, M., Deng, Y., Jing, W., and Yang, J.: Factors Influencing O3 Concentration in Traffic and Urban Environments: A Case Study of Guangzhou City, Int. J. Environ. Res. Public Health, 19, 12961, https://doi.org/10.3390/ijerph191912961, 2022a.

Liu, Y., Wu, S., Chen, H., Federici, M., Perricone, G., Li, Y., Lv, G., Munir, S., Luo, Z., and Mao, B.: Brake wear induced PM10 emissions during the world harmonised light-duty vehicle test procedure-brake cycle, J. Cleaner Prod., 361, 132278, https://doi.org/10.1016/j.jclepro.2022.132278, 2022b.

Lopez, B., Wang, X., Chen, L.-W. A., Ma, T., Mendez-Jimenez, D., Cobb, L. C., Frederickson, C., Fang, T., Hwang, B., Shiraiwa, M., Park, M., Park, K., Yao, Q., Yoon, S., and Jung, H.: Metal contents and size distributions of brake and tire wear particles dispersed in the near-road environment, Sci. Total Environ., 883, 163561, https://doi.org/10.1016/j.scitotenv.2023.163561, 2023.

Lüchtrath, S., Wutke, R., and Held, A.: Secondary Formation of Light-Absorbing, Insoluble Particles from Catechol in the Presence of Fe(II) or Fe(III) and Hydrogen Peroxide at Dark and Light Conditions, ACS ES&T Air, 2, 2365–2375, https://doi.org/10.1021/acsestair.5c00091, 2025.

Luoma, K., Niemi, J. V., Aurela, M., Fung, P. L., Helin, A., Hussein, T., Kangas, L., Kousa, A., Rönkkö, T., Timonen, H., Virkkula, A., and Petäjä, T.: Spatiotemporal variation and trends in equivalent black carbon in the Helsinki metropolitan area in Finland, Atmos. Chem. Phys., 21, 1173–1189, https://doi.org/10.5194/acp-21-1173-2021, 2021.

Lyu, Y. and Olofsson, U.: On black carbon emission from automotive disc brakes, J. Aerosol Sci., 148, 105610, https://doi.org/10.1016/j.jaerosci.2020.105610, 2020.

Magee Scientific: Aethalometer® Model AE33 User's Manual, Version 1.70, Aerosol d.o.o., Ljubljana, Slovenia, https://aerosolmageesci.com/wp-content/uploads/2025/05/AE33_UsersManual_Rev170_A4-1.pdf, 2024.

Malik, A. and Aggarwal, S. G.: A Review on the Techniques Used and Status of Equivalent Black Carbon Measurement in Two Major Asian Countries, Asian J. Atmos. Environ., 15, 2021044, https://doi.org/10.5572/ajae.2021.044, 2021.

Meyer, H., Kandler, K., Dupont, S., Escribano, J., Girdwood, J., Nikolich, G., Alastuey, A., Etyemezian, V., González-Flórez, C., González-Romero, A., Hussein, T., Irvine, M., Knippertz, P., Möhler, O., Querol, X., Stopford, C., Vogel, F., Weis, F., Wieser, A., Pérez García-Pando, C., and Klose, M.: From fine to giant: multi-instrument assessment of the dust particle size distribution at an emission source during the J-WADI field campaign, Atmos. Meas. Tech., 19, 21–61, https://doi.org/10.5194/amt-19-21-2026, 2026.

Mishra, K. G., Izhar, S., Paul, D., Qadri, A. M., and Gupta, T.: Insights on optical absorption and isotopic properties of carbonaceous aerosol in PM2.5 and PM10 from different emission sources, Environ. Pollut., 382, 126558, https://doi.org/10.1016/j.envpol.2025.126558, 2025.

Moteki, N.: Climate-relevant properties of black carbon aerosols revealed by in situ measurements: a review, Prog. Earth Planet Sci., 10, 12, https://doi.org/10.1186/s40645-023-00544-4, 2023.

Müller, T., Henzing, J. S., de Leeuw, G., Wiedensohler, A., Alastuey, A., Angelov, H., Bizjak, M., Collaud Coen, M., Engström, J. E., Gruening, C., Hillamo, R., Hoffer, A., Imre, K., Ivanow, P., Jennings, G., Sun, J. Y., Kalivitis, N., Karlsson, H., Komppula, M., Laj, P., Li, S.-M., Lunder, C., Marinoni, A., Martins dos Santos, S., Moerman, M., Nowak, A., Ogren, J. A., Petzold, A., Pichon, J. M., Rodriquez, S., Sharma, S., Sheridan, P. J., Teinilä, K., Tuch, T., Viana, M., Virkkula, A., Weingartner, E., Wilhelm, R., and Wang, Y. Q.: Characterization and intercomparison of aerosol absorption photometers: result of two intercomparison workshops, Atmos. Meas. Tech., 4, 245–268, https://doi.org/10.5194/amt-4-245-2011, 2011.

Peng, J., Hu, M., Guo, S., Du, Z., Zheng, J., Shang, D., Levy Zamora, M., Zeng, L., Shao, M., Wu, Y.-S., Zheng, J., Wang, Y., Glen, C. R., Collins, D. R., Molina, M. J., and Zhang, R.: Markedly enhanced absorption and direct radiative forcing of black carbon under polluted urban environments, Proc. Natl. Acad. Sci. U.S.A., 113, 4266–4271, https://doi.org/10.1073/pnas.1602310113, 2016.

Petzold, A. and Schönlinner, M.: Multi-angle absorption photometry—a new method for the measurement of aerosol light absorption and atmospheric black carbon, J. Aerosol Sci., 35, 421–441, https://doi.org/10.1016/j.jaerosci.2003.09.005, 2004.

Pu, W., Wang, X., Zhang, X., Ren, Y., Shi, J.-S., Bi, J.-R., and Zhang, B.-D.: Size Distribution and Optical Properties of Particulate Matter (PM10) and Black Carbon (BC) during Dust Storms and Local Air Pollution Events across a Loess Plateau Site, Aerosol Air Qual. Res., 15, 2212–2224, https://doi.org/10.4209/aaqr.2015.02.0109, 2015.

Remoundaki, E., Bourliva, A., Kokkalis, P., Mamouri, R. E., Papayannis, A., Grigoratos, T., Samara, C., and Tsezos, M.: PM10 composition during an intense Saharan dust transport event over Athens (Greece), Sci. Total Environ., 409, 4361–4372, https://doi.org/10.1016/j.scitotenv.2011.06.026, 2011.

Reynolds, R. L., Molden, N., Kokaly, R. F., Lowers, H., Breit, G. N., Goldstein, H. L., Williams, E. K., Lawrence, C. R., and Derry, J.: Microplastic and Associated Black Particles From Road-Tire Wear: Implications for Radiative Effects Across the Cryosphere and in the Atmosphere, J. Geophys. Res. Atmos., 129, e2024JD041116, https://doi.org/10.1029/2024JD041116, 2024.

Rönkkö, T., Saarikoski, S., Kuittinen, N., Karjalainen, P., Keskinen, H., Järvinen, A., Mylläri, F., Aakko-Saksa, P., and Timonen, H.: Review of black carbon emission factors from different anthropogenic sources, Environ. Res. Lett., 18, 033004, https://doi.org/10.1088/1748-9326/acbb1b, 2023.

Rovira, J., Savadkoohi, M., Chen, G. I., Močnik, G., Aas, W., Alados-Arboledas, L., Artiñano, B., Aurela, M., Backman, J., Banerji, S., Beddows, D., Brem, B., Chazeau, B., Coen, M. C., Colombi, C., Conil, S., Costabile, F., Coz, E., de Brito, J. F., Eleftheriadis, K., Favez, O., Flentje, H., Freney, E., Gregorič, A., Gysel-Beer, M., Harrison, R., Hueglin, C., Hyvärinen, A., Ivančič, M., Kalogridis, A.-C., Keernik, H., Konstantinos, G., Laj, P., Liakakou, E., Lin, C., Listrani, S., Luoma, K., Maasikmets, M., Manninen, H. E., Marchand, N., dos Santos, S. M., Mbengue, S., Mihalopoulos, N., Nicolae, D., Niemi, J. V., Norman, M., Ovadnevaite, J., Petit, J.-E., Platt, S., Prévôt, A. S. H., Pujadas, M., Putaud, J.-P., Riffault, V., Rigler, M., Rinaldi, M., Schwarz, J., Silvergren, S., Teinemaa, E., Teinilä, K., Timonen, H., Titos, G., Tobler, A., Vasilescu, J., Vratolis, S., Yttri, K. E., Yubero, E., Zíková, N., Alastuey, A., Petäjä, T., Querol, X., Yus-Díez, J., and Pandolfi, M.: A European aerosol phenomenology – 9: Light absorption properties of carbonaceous aerosol particles across surface Europe, Environ. Int., 195, 109185, https://doi.org/10.1016/j.envint.2024.109185, 2025.

Saarikoski, S., Hellén, H., Praplan, A. P., Schallhart, S., Clusius, P., Niemi, J. V., Kousa, A., Tykkä, T., Kouznetsov, R., Aurela, M., Salo, L., Rönkkö, T., Barreira, L. M. F., Pirjola, L., and Timonen, H.: Characterization of volatile organic compounds and submicron organic aerosol in a traffic environment, Atmos. Chem. Phys., 23, 2963–2982, https://doi.org/10.5194/acp-23-2963-2023, 2023.

Saha, P. K., Khlystov, A., Snyder, M. G., and Grieshop, A. P.: Characterization of air pollutant concentrations, fleet emission factors, and dispersion near a North Carolina interstate freeway across two seasons, Atmos. Environ., 177, 143–153, https://doi.org/10.1016/j.atmosenv.2018.01.019, 2018.

Salo, L., Hyvärinen, A., Jalava, P., Teinilä, K., Hooda, R. K., Datta, A., Saarikoski, S., Lintusaari, H., Lepistö, T., Martikainen, S., Rostedt, A., Sharma, V. P., Rahman, Md. H., Subudhi, S., Asmi, E., Niemi, J. V., Lihavainen, H., Lal, B., Keskinen, J., Kuuluvainen, H., Timonen, H., and Rönkkö, T.: The characteristics and size of lung-depositing particles vary significantly between high and low pollution traffic environments, Atmos. Environ., 255, 118421, https://doi.org/10.1016/j.atmosenv.2021.118421, 2021.

Salo, L., Saarnio, K., Saarikoski, S., Teinilä, K., Barreira, L. M. F., Marjanen, P., Martikainen, S., Keskinen, H., Mustonen, K., Lepistö, T., Aakko-Saksa, P., Hakkarainen, H., Pfeiffer, T., Jalava, P., Karjalainen, P., Keskinen, J., Kuittinen, N., Timonen, H., and Rönkkö, T.: Black carbon instrument responses to laboratory generated particles, Atmos. Pollut. Res., 15, 102088, https://doi.org/10.1016/j.apr.2024.102088, 2024.

Sandradewi, J., Prévôt, A. S. H., Szidat, S., Perron, N., Alfarra, M. R., Lanz, V. A., Weingartner, E., and Baltensperger, U.: Using Aerosol Light Absorption Measurements for the Quantitative Determination of Wood Burning and Traffic Emission Contributions to Particulate Matter, Environ. Sci. Technol., 42, 3316–3323, https://doi.org/10.1021/es702253m, 2008.

Savadkoohi, M., Pandolfi, M., Alastuey, A., Petäjä, T., Putaud, J. P., Favez, O., and Querol, X.: Guidance documents on measurements & modelling of novel air quality pollutants: Black carbon (BC) determinations, RI-URBANS, https://riurbans.eu/wp-content/uploads/2024/10/GUIDANCE-DOCUMENT_ST2_BC_Definitive.pdf, 2024.

Schuster, G. L., Dubovik, O., and Holben, B. N.: Angstrom exponent and bimodal aerosol size distributions, J. Geophys. Res. Atmos., 111, https://doi.org/10.1029/2005JD006328, 2006.

Stojiljkovic, A., Kauhaniemi, M., Kukkonen, J., Kupiainen, K., Karppinen, A., Denby, B. R., Kousa, A., Niemi, J. V., and Ketzel, M.: The impact of measures to reduce ambient air PM_{10} concentrations originating from road dust, evaluated for a street canyon in Helsinki, Atmos. Chem. Phys., 19, 11199–11212, https://doi.org/10.5194/acp-19-11199-2019, 2019.

The jamovi project: jamovi (Version 2.7) [Computer Software], https://www.jamovi.org/about.html, 2026.

Thorpe, A. and Harrison, R. M.: Sources and properties of non-exhaust particulate matter from road traffic: a review, Sci. Total Environ., 400, 270–282, https://doi.org/10.1016/j.scitotenv.2008.06.007, 2008.

Tohidi, R., Farahani, V. J., and Sioutas, C.: Real-time measurements of mineral dust concentration in coarse particulate matter (PM10-2.5) by employing a novel optical-based technique in Los Angeles, Sci. Total Environ., 838, 156215, https://doi.org/10.1016/j.scitotenv.2022.156215, 2022.

Utry, N., Ajtai, T., Filep, Á., Pintér, M., Török, Zs., Bozóki, Z., and Szabó, G.: Correlations between absorption Angström exponent (AAE) of wintertime ambient urban aerosol and its physical and chemical properties, Atmos. Environ., 91, 52–59, https://doi.org/10.1016/j.atmosenv.2014.03.047, 2014.

Virkkula, A.: Modeled source apportionment of black carbon particles coated with a light-scattering shell, Atmos. Meas. Tech., 14, 3707–3719, https://doi.org/10.5194/amt-14-3707-2021, 2021.

Virkkula, A., Mäkelä, T., Hillamo, R., Yli-Tuomi, T., Hirsikko, A., Hämeri, K., and Koponen, I. K.: A Simple Procedure for Correcting Loading Effects of Aethalometer Data, J. Air Waste Manage. Assoc., 57, 1214–1222, https://doi.org/10.3155/1047-3289.57.10.1214, 2007.

Wagner, S., Funk, C. W., Müller, K., and Raithel, D. J.: The chemical composition and sources of road dust, and of tire and road wear particles–A review, Sci. Total Environ., 926, 171694, https://doi.org/10.1016/j.scitotenv.2024.171694, 2024.

Wang, J., Wang, S., Wang, J., Hua, Y., Liu, C., Cai, J., Xu, Q., Xu, X., Jiang, S., Zheng, G., Jiang, J., Cai, R., Zhou, W., Chen, G., Jin, Y., Zhang, Q., and Hao, J.: Significant Contribution of Coarse Black Carbon Particles to Light Absorption in North China Plain, Environ. Sci. Technol. Lett., 9, 134–139, https://doi.org/10.1021/acs.estlett.1c00953, 2022.

Wei, Y. and Kumar, P.: Beyond the tailpipe: Review of non-exhaust airborne nanoparticles from road vehicles, Eco-Environ. Health, 4, 100130, https://doi.org/10.1016/j.eehl.2024.11.003, 2024.

Weingartner, E., Saathoff, H., Schnaiter, M., Streit, N., Bitnar, B., and Baltensperger, U.: Absorption of light by soot particles: determination of the absorption coefficient by means of aethalometers, J. Aerosol Sci., 34, 1445–1463, https://doi.org/10.1016/S0021-8502(03)00359-8, 2003.

Xie, M., Chen, X., Hays, M. D., Lewandowski, M., Offenberg, J., Kleindienst, T. E., and Holder, A. L.: Light Absorption of Secondary Organic Aerosol: Composition and Contribution of Nitroaromatic Compounds, Environ. Sci. Technol., 51, 11607–11616, https://doi.org/10.1021/acs.est.7b03263, 2017.

Yus-Díez, J., Bernardoni, V., Močnik, G., Alastuey, A., Ciniglia, D., Ivančič, M., Querol, X., Perez, N., Reche, C., Rigler, M., Vecchi, R., Valentini, S., and Pandolfi, M.: Determination of the multiple-scattering correction factor and its cross-sensitivity to scattering and wavelength dependence for different AE33 Aethalometer filter tapes: a multi-instrumental approach, Atmos. Meas. Tech., 14, 6335–6355, https://doi.org/10.5194/amt-14-6335-2021, 2021.

Yus-Díez, J., Escribano, J., Pandolfi, M., Alastuey, A., González-Flórez, C., Gonzalez-Romero, A., Gonçalves Ageitos, M., Ivančič, M., Klose, M., Kandler, K., Obiso, V., Panta, A., Reche, C., Rigler, M., Querol, X., and Perez Garćia-Pando, C.: Optical Properties and Shape-Dependent Complex Refractive Index Retrievals of Freshly Emitted Saharan Dust, EGUsphere, 1–32, https://doi.org/10.5194/egusphere-2025-2571, 2025.

Zhang, G., Peng, L., Lian, X., Lin, Q., Bi, X., Chen, D., Li, M., Li, L., Wang, X., and Sheng, G.: An Improved Absorption Ångström Exponent (AAE)-Based Method for Evaluating the Contribution of Light Absorption from Brown Carbon with a High-Time Resolution, Aerosol Air Qual. Res., 19, 15–24, https://doi.org/10.4209/aaqr.2017.12.0566, 2019.

Zhang, J., Wu, L., Fang, X., Li, F., Yang, Z., Wang, T., Mao, H., and Wei, E.: Elemental Composition and Health Risk Assessment of PM10 and PM2.5 in the Roadside Microenvironment in Tianjin, China, Aerosol Air Qual. Res., 18, 1817–1827, https://doi.org/10.4209/aaqr.2017.10.0383, 2018.

Zhang, Q., Fang, T., Yin, J., Men, Z., Peng, J., Wu, L., and Mao, H.: Vehicle Non-Exhaust Emissions Significantly Contribute to Urban PM Pollution in New Energy Vehicles Era, J. Geophys. Res. Atmos., 130, e2024JD042126, https://doi.org/10.1029/2024JD042126, 2025.

Zhang, X. L., Wu, G. J., Zhang, C. L., Xu, T. L., and Zhou, Q. Q.: What is the real role of iron oxides in the optical properties of dust aerosols?, Atmos. Chem. Phys., 15, 12159–12177, https://doi.org/10.5194/acp-15-12159-2015, 2015.

Zhang, X. Y., Wang, Y. Q., Zhang, X. C., Guo, W., Niu, T., Gong, S. L., Yin, Y., Zhao, P., Jin, J. L., and Yu, M.: Aerosol monitoring at multiple locations in China: contributions of EC and dust to aerosol light absorption, Tellus B: Chem. Phys. Meteorol., 60, 647–656, https://doi.org/10.1111/j.1600-0889.2008.00359.x, 2008.

Zheng, H., Kong, S., Ding, D., Savadkoohi, M., Song, C., Zheng, M., and Harrison, R. M.: Black carbon aerosols in China: spatial-temporal variations and lessons from long-term atmospheric observations, Atmos. Chem. Phys., 25, 16363–16386, https://doi.org/10.5194/acp-25-16363-2025, 2025.

Zioła, N., Błaszczak, B., and Klejnowski, K.: Long-Term eBC Measurements with the Use of MAAP in the Polluted Urban Atmosphere (Poland), Atmosphere, 12, https://doi.org/10.3390/atmos12070808, 2021.